2-9-2010

Polarization diverse tracking antenna with high sensitivity

Michael Pace

Michael T. Pace
Candidate

Electrical and Computer Engineering
Department

This thesis is approved, and it is acceptable in quality and form for publication:

Approved by the Thesis Committee:

Dr. Christos Christodoulou, Chairperson

Dr. Mark Gilmore, Committee Member

Dr. Edl Schamiloglu, Committee Member

POLARIZATION DIVERSE TRACKING ANTENNA WITH HIGH SENSITIVITY

by

Michael T. Pace

B.S., Electrical Engineering,

New Mexico Institute of Mining and Technology, 2007

THESIS

Submitted in Partial Fulfillment of the
Requirements for the Degree of

Master of Science

Electrical Engineering

The University of New Mexico
Albuquerque, New Mexico

December, 2009

ACKNOWLEDGMENTS

First of all, I thank God for giving me the passion to work in the field of electromagnetics. My advisor, Dr. Christodoulou, has helped me along the way to complete this thesis. I greatly appreciate his time spent on edits and revisions. I would also like to thank my committee members for taking the time to review my work. Mrs. Elmyra Grelle, the Coordinator of Graduate program for the ECE department, deserves acknowledgement for helping me complete all of the required paperwork and encouraging me throughout the program.

This thesis would not have been possible without the support of the Ktech Corporation in Albuquerque, NM. I would also like to thank the Field Test Department at Ktech for their contributions to the HSDTA. Specific accolades go out to my peer editors of my thesis: Michael Petty and Andy Lewis for meticulously editing the manuscript over the last few months. Finally, I would like to thank my wife and family for always being there to encourage and inspire me throughout my schooling.

POLARIZATION DIVERSE TRACKING ANTENNA WITH HIGH SENSITIVITY

Prepared by:

Michael T. Pace

B.S., Electrical Engineering,
New Mexico Institute of Mining and Technology, 2007

THESIS

Submitted in Partial Fulfillment of the
Requirements for the Degree of

Master of Science

Electrical Engineering

The University of New Mexico
Albuquerque, New Mexico

December, 2009

POLARIZATION DIVERSE TRACKING ANTENNA WITH HIGH SENSITIVITY

by

Michael T. Pace

ABSTRACT OF THESIS

Submitted in Partial Fulfillment of the
Requirements for the Degree of

Master of Science

Electrical Engineering

The University of New Mexico
Albuquerque, New Mexico

December, 2009

POLARIZATION DIVERSE TRACKING ANTENNA WITH HIGH SENSITIVITY

by

Michael T. Pace

B.S.E.E, New Mexico Institute of Mining and Technology, 2007
M.S.E.E, University of New Mexico, 2009

ABSTRACT

The design of an S-band aperture coupled microstrip antenna array for use on airborne telemetry platforms is presented. The High Sensitivity Diverse Tracking Antenna (HSDTA) is capable of receiving both left and right hand circular polarizations and has RF auto-tracking capability. Novel placement of RF terminations throughout the design allows for HSDTA to be installed in multiple configurations aboard different airborne platforms while maintaining consistent mechanical mobility and high sensitivity. The HSDTA was successfully simulated, fabricated, and deployed. Measured RF performance, including the operational bandwidth, gain, and sensitivity, are discussed and compared to the simulation. The HSDTA was designed to withstand the environmental conditions present while flying at altitude. The system has been successfully used to collect telemetry while deployed on an airborne platform flying over the South Pacific at 35000 ft.

Table of Contents

CHAPTER 1

Introduction

1.1. Introduction

The most important component of an airborne telemetry platform is the antenna system. In order to collect telemetry data with high fidelity, the antenna system must be capable of receiving and amplifying small amplitude signals without introducing significant amounts of noise. Additionally, the antenna system must be sensitive to both the frequency and the polarization of the source signal. The link margin of the telemetry stream can be further improved if polarization diversity is used. Polarization diversity can only be implemented if the receiving antenna system can simultaneously receive two polarization senses. In the absence of externally supplied tracking data an antenna system which is capable of auto-tracking the target further augments the capabilities of the telemetry platform.

Very few off-the-shelf antenna systems exist which meet all system requirements while remaining flexible enough to be quickly integrated on different aircraft. In an environment where both the aircraft and the target are dynamically moving, a mechanical pedestal is typically used to maintain proper pointing of the antenna system. The pedestal must be installed within a radome on the aircraft to block the flow of air and protect the antenna from the environment. The radomes on different airborne platforms vary; thus, the size of the antenna must be customized for each aircraft. In an industry where it is possible to use a different aircraft for each mission, the proposition of creating a unique antenna for every mission is complicated, cost restrictive, and risky. This thesis proposes the design of a single antenna system which can be modified to fit on any aircraft.

The High Sensitivity Diverse Tracking Antenna (HSDTA) consists of an active planar array of microstrip elements which are fed by a network of Low Noise Amplifiers (LNA) and equal amplitude and phase power dividers. Each array element is capable of receiving both orthogonal linear polarizations. When each polarization is fed by a hybrid coupler, the HSDTA is capable of receiving both senses of circular polarization. The HSDTA is laid out into four quadrants which simplifies the design of the array and allows for RF auto-tracking capability. Strategic placement of unpopulated RF terminations throughout the array allow for the design to be modified, without compromising the integrity of the feed network. Having this flexibility allows the HSDTA to be customized for different airborne assets while maximizing the available array size.

1.2. System Requirements

The basic required design goals for the HSDTA are listed below.

- Sensitive to Right Hand Circular (RHCP) and Left Hand Circular (LHCP) Polarization senses
- Maximum physical dimensions defined by a 34” diameter, 1” thick cylinder
- Capable of generating RF auto-tracking signals
- S11 under -10 dB from 2.2 to 2.4 GHz
- A realized gain of 21 dBi at mid-band
- Operating temperatures of -50° C to +80° C.
- A G/T of 3 dB/K at mid-band

Additionally, the following design goals were desired:

- A realized gain of 25 dB or greater at mid-band (2.3 GHz)
- A G/T of 3.5 dB/K at mid-band
- Overall weight of under 50 lbs
- A flexible design that can be easily modified for multiple aircraft radomes

The antenna system must be able to withstand the environmental conditions outside of the pressure vessel on an aircraft at 40,000 ft and have the capability to RF auto-track when paired with an auto-tracking receiver (ATR) and an antenna control unit (ACU).

1.3. Thesis Organization

The organization of the thesis follows the design process used for the HSDTA. The thesis will begin by presenting two different base antenna candidates for the HSDTA design: the rectangular microstrip patch antenna and the circular microstrip patch antenna. For each candidate, relevant design parameters will be discussed. The modes supported by each candidate will be discussed and compared to polarization capabilities.

With a base antenna element chosen, the thesis will discuss an aperture coupled feed network for the selected candidate. Additionally, the active components of the selected element will be discussed. This will include a discussion on the importance of locating low noise amplifiers at the feed of the antenna to meet the G/T requirements. To meet the requirement of auto-tracking, mono-pulse and electronically scanned auto-tracking configurations will also be discussed.

The thesis will then present antenna array theory and the final array design of the HSDTA. The HSDTA was simulated and optimized in CST Microwave Studio prior to fabrication; the results of the computer simulation will be discussed along with the optimization. The thesis will then discuss how the HSDTA was fabricated using a novel composition of microwave materials to decrease the overall thickness of the antenna while satisfying all design requirements.

The results from the fully fabricated and tested HSDTA will be discussed including a non-standard method of measuring an active array's S11 parameters. The results from an open air antenna range farfield radiation patterns and gain measurement will be compared with simulated results and similarities will be discussed. The measurement of the system noise temperature by two methods will also be discussed which leads to the estimated antenna Gain over Temperature (G/T) figure of merit.

Finally, the thesis summarizes future work and lessons learned from the design of the HSDTA. The results of airborne testing of the HSDTA will also be discussed.

CHAPTER 2

Design Approach

The design of the HSDTA began with the design and simulation of a base antenna element for the array including the aperture coupled feed network (ACF). Next, a series of low noise amplifiers and equal amplitude and phase power dividers were designed in order to provide the necessary feed network for the array. Once the base antenna element was completed, a single quadrant of the array was modeled and simulated.

With a quadrant of the array optimized, the design was transferred into a Printed Circuit Board (PCB) layout software suite where the DC components were added. Finally, the array was fabricated and tested.

2.1. Microstrip Patch Antennas

2.1.1. Rectangular Patch

The most common microstrip patch antenna element is the rectangular patch. The patch consists of a very thin sheet of metal which is located on top of a dielectric substrate of thickness “h”. On the opposite side of the substrate is a ground plane. The basic rectangular microstrip patch structure can be seen below in Figure 1.

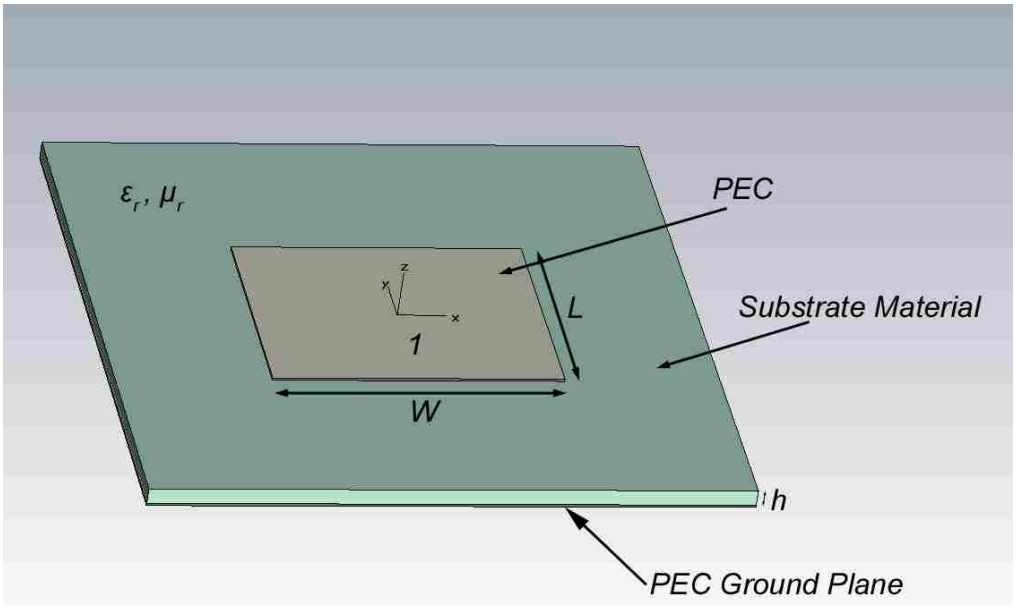

Figure 1: Basic rectangular microstrip patch configuration.

The area between the patch and the ground plane form can be modeled as a cavity which supports several different electric field configurations or modes. When properly excited by the fundamental mode, the rectangular patch radiates from the top and bottom edges as can be seen in Figure 2. If the length *L* is such that the separation between these two edges is λ/2, then the total radiated fields of the patch will be broadside (normal) to the surface of the metallic patch (See Figure 3).

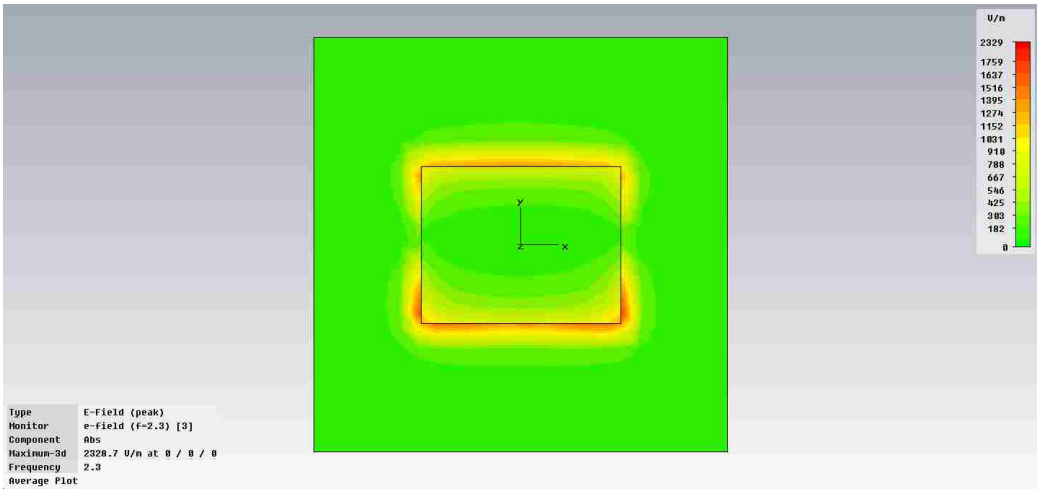

Figure 2: Time average of the Electric fields present on a rectangular patch.

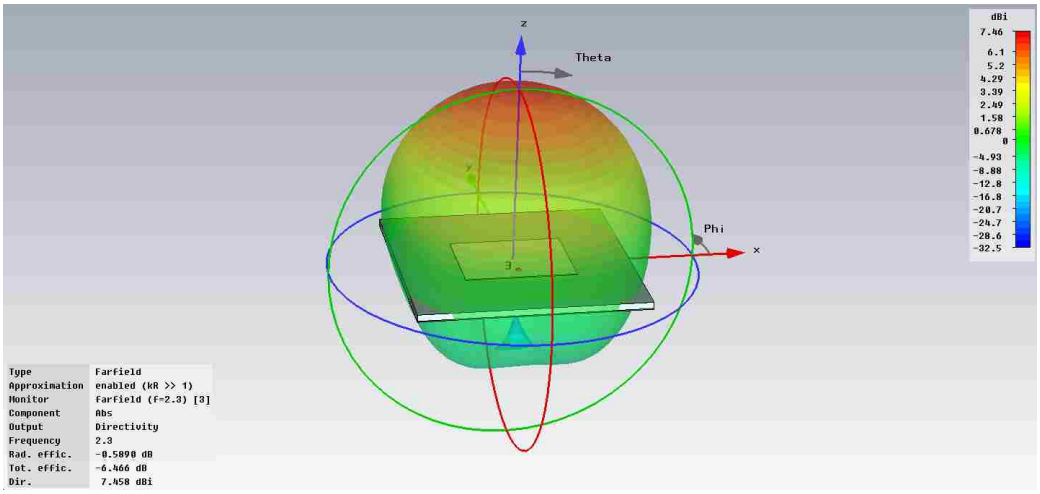

Figure 3: Farfield radiation pattern of a probe feed rectangular patch antenna.

In order to determine the optimal dimensions of the patch, one must first specify the substrate material's dielectric constant and thickness as well as the desired resonant frequency [8]. The next step is to determine the width of patch as defined by [6]:

$$W = \frac{C}{2f_r}\sqrt{\frac{2}{\varepsilon_r + 1}} \tag{1}$$

With:

C	=	Speed of light
ε_r	=	Dielectric constant of substrate

Once the width has been determined by (1), one must find the effective dielectric constant of the substrate. Note, this is different from the material dielectric constant due to the effects of fringing [8] and is defined by [7]:

$$\varepsilon_{reff} = \frac{\varepsilon_r + 1}{2} + \frac{\varepsilon_r - 1}{2}\left[1 + 12\frac{h}{W}\right]^{-1/2} \tag{2}$$

Also due to the effects of fringing, the electrical length of the patch differs from the physical length and is defined by [9]:

$$\Delta L = 0.412h\frac{\left(\varepsilon_{reff}+0.3\right)\left(\frac{W}{h}+0.264\right)}{\left(\varepsilon_{reff}-0.258\right)\left(\frac{W}{h}+0.8\right)} \tag{3}$$

The length of the patch is determined by using the following approximation [8]:

$$L = \frac{C}{2f_r\sqrt{\varepsilon_{reff}}} - 2\Delta L \tag{4}$$

With:

C	=	Speed of light
ε_{reff}	=	Effective dielectric constant of substrate

It is clear that (4) takes into account both the decrease in wavelength due to the effective dielectric constant of the substrate and the effects of fringing on the electrical length patch. The polarization of a rectangular patch is linear and parallel to the "L" dimension of the patch. To implement dual polarization using a rectangular patch, two patches must be used which are placed orthogonally to each other. This design adds complexity and space to the array; therefore, it was not selected for the HSDTA.

A circular patch with two feeds will support two separate modes and will generate two orthogonal polarizations. The circular patch was selected for this design and is presented in the following section.

2.1.2. Circular Patch

Similar to the rectangular patch, the circular patch consists of a circular metallic disk located above a ground plane on a dielectric substrate of thickness “h” (Figure 4).

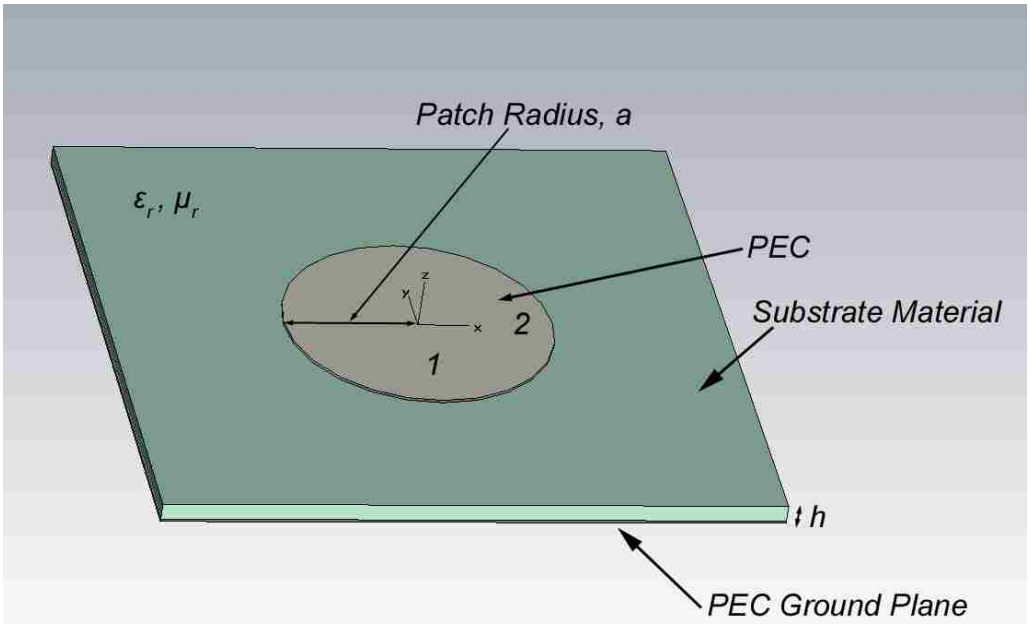

Figure 4: The structure of a circular microstrip patch.

The resonate frequency of the circular patch varies with the radius of the patch while the impedance bandwidth of the patch varies with the feed location. Assuming the cavity formed by the circular patch is in the dominate TM_{110} mode, the resonate frequency of the patch is given by [8]:

$$f_r = \frac{1.8412C}{a_e 2\pi\sqrt{\varepsilon_r}} \tag{5}$$

$$a_e = a\sqrt{1+\frac{2h}{a\pi\varepsilon_r}\left[\ln\left(\frac{a\pi}{2h}+1.7726\right)\right]} \tag{6}$$

With:

a	=	radius of patch
h	=	height of substrate
C	=	Speed of light
ε_r	=	Dielectric constant of substrate

When the circular patch is fed properly, the edges of the patch will act as slot radiators as can be seen below in Figure 5. If the radius of the patch is dictated by (5, 6), then the radiation from the two edges will add in phase in the farfield.

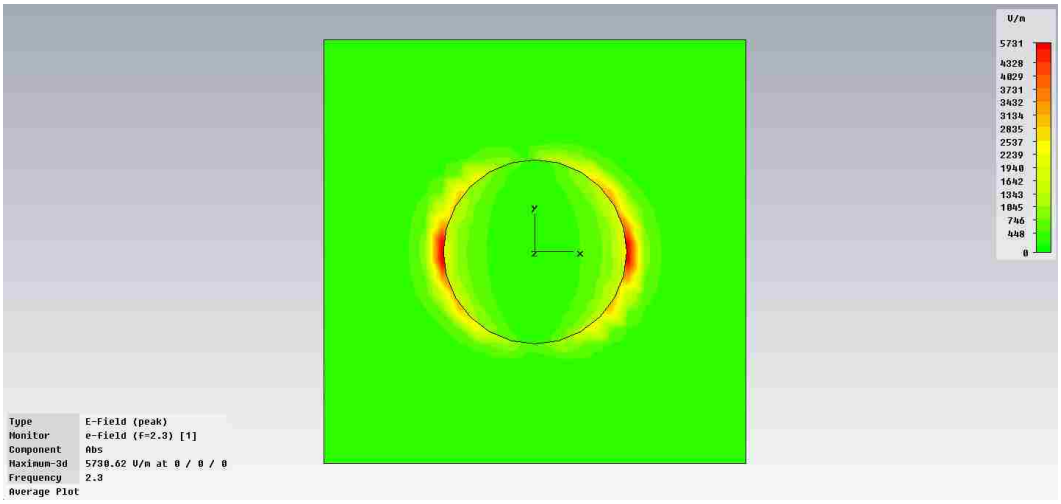

Figure 5: Average electric field for a horizontally fed circular patch.

The circular patch was designed to operate in the fundamental TM_{110} mode. In order to generate dual polarization, the circular patch was fed at two orthogonal locations. By placing the feeds 90° apart, the nulls of one

TM_{110} mode are located at the maxima for the other TM_{110} mode which provides isolation between the feeds (See Figures 5 & 6). By exciting the circular patch in this manner, the structure will also simultaneously generate two orthogonal linear polarizations. Co-locating both linear polarizations on a single antenna element helps to reduce the overall size of the array and allows for more array elements per polarization to be used, which increases the efficiency of the array. For applications which require circular polarizations, one must simply allow a 90° phase shift between the feed ports.

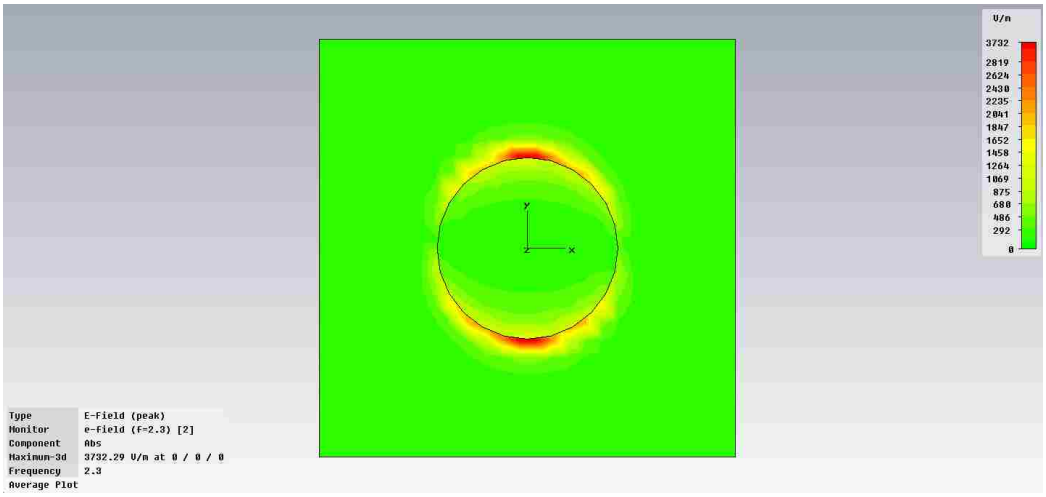

Figure 6: Average electric field for a vertically fed circular patch.

The bandwidth of the circular patch is primarily dictated by the substrate thickness and the dielectric constant (ε_r) of the substrate material. As can be seen in Figure 7, the bandwidth of the patch increases both as the thickness of the substrate increases and as ε_r decreases [25].

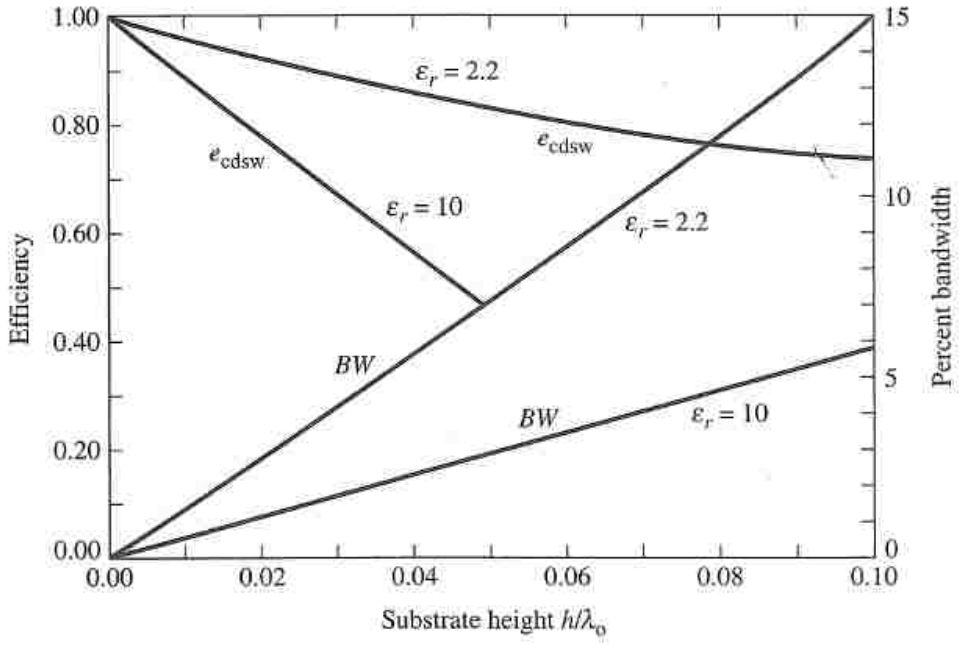

Figure 7: Plot showing patch bandwidth variations versus substrate height and dielectric constant [25].

The desired antenna system must operate from 2.2 to 2.4 GHz. With a center frequency of 2.3 GHz, the operational bandwidth must be 200MHz or 8.69%. At the center frequency the wavelength is: λ_c = 13.04 cm. Based on Figure7, if a substrate ε_r of 2.2 was selected, in order to get ~9% bandwidth, the thickness of the substrate would have to be on the order of 9.4 mm or 0.370". While it is possible to fabricate a board with these dimensions, the board would be complicated and cost restrictive; therefore, another technique needs to be investigated.

The primary options were to either increase the substrate thickness or lower the dielectric constant of the substrate. The ideal case for bandwidth enhancement would be a thick air dielectric. While this method of gaining bandwidth has been used in several places, [16]-[19] it is typically used in applications where the overall thickness of the array is not a major constraint on the design. Another popular technique uses a foam substrate to separate the patch and feed boards [11][21]-[23]. For S-band,

where the antenna structure is large relative to the design constraints, a foam dielectric was chosen which has very similar electrical properties to air. The foam has a very low ε_r of 1.03 and an extremely low loss tangent of 0.0001. The foam also provides additional structural support for the patch layer and allows the top and bottom PCBs to be bonded together using adhesives.

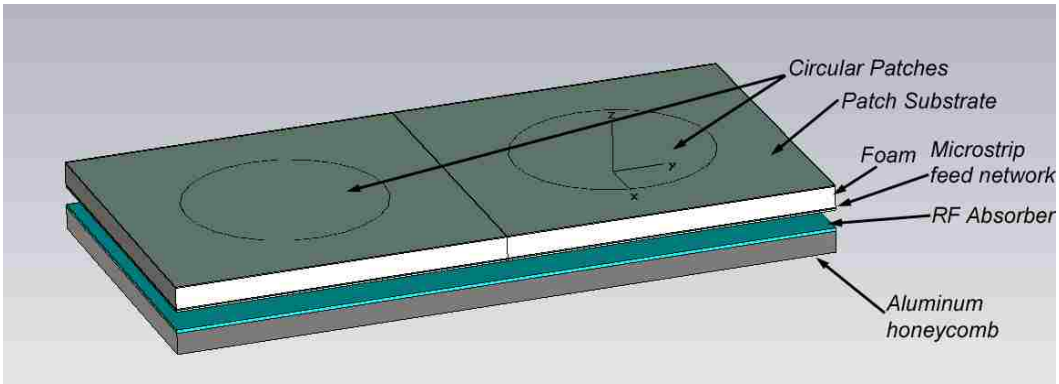

Figure 8: The layers of the HSDTA.

The final stack up of the antenna can be seen in Figure 8. The circular patch is printed on a thin (12mil) substrate of microwave material. This top board is located on a layer of PP-2 foam. Following the foam layer is the antenna back-end board which contains the antenna feed structure, LNAs, and the DC components of the HSDTA. In order to meet the structure requirements for airborne applications, the antenna was mounted onto an aluminum honeycomb support structure. The aluminum honeycomb provides the stiffness of a solid plate without the added weight. Since the antenna structure was limited to an overall height of 1", the dimensions between the aluminum honeycomb and the feed network which is located on the antenna backend board are small. The proximity of this metal structure to the feed network led to mutual coupling issues and RF interference between the different feed lines on the back of the antenna backend board. To fix this problem, the aluminum honeycomb structure was lined with a low profile RF absorber. The absorber cuts down on the

reflections off the metallic surface by nearly 30dB at mid-band and successfully eliminated mutual coupling between the feed lines on the antenna backend board and the aluminum honeycomb.

2.2. Feed Network

There are several methods of feeding a microstrip antenna. Some of the more common feeding techniques are: recessed microstrip, offset microstrip, coaxial, proximity coupling, and aperture coupling. The HSDTA requires a feed network which supports both the thick substrate as well as the extended bandwidth of the patch. The aperture coupled feed (ACF) was chosen because it is capable of supporting bandwidths on the order of 10% and it is innately compatible with the multilayer stack-up of the HSDTA. The small size and geometric layout of the ACF allows for two ACFs to be located close to each other. This allows for a dual polarization feed for each patch element.

The ACF does not require a direct connection between the patch on the top layer and the feed lines on the bottom layer. Due to this freedom, the material between the patch and the feed line can be a thick composite of multiple materials.

2.2.1. Single Element, Dual Polarization

In order to have dual polarization, the feed network must excited two orthogonal modes of the patch while maintaining isolation between the two feed lines. It is also important that the feed structure is capable of supporting the entire bandwidth of the patch. By modifying the shape of the slot in the ground plane to an H-Slot, one is able to increase the coupling and operational bandwidth of the feed network while maintaining isolation between the two ports and thus lowers the axial ratio of the

antenna [5]. It was also important that the feed network was symmetric per antenna element pair without having a phase or amplitude imbalance. This symmetry also makes the layout of the array simpler. The final feed of a single antenna element can be seen below in Figure 9.

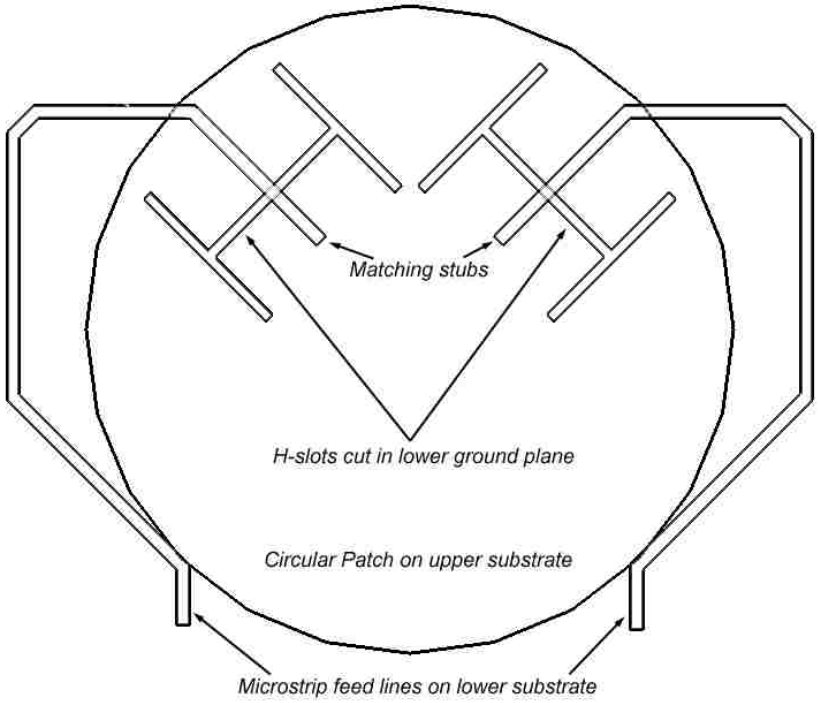

Figure 9: Dual polarization aperture coupled feed for the circular patch.

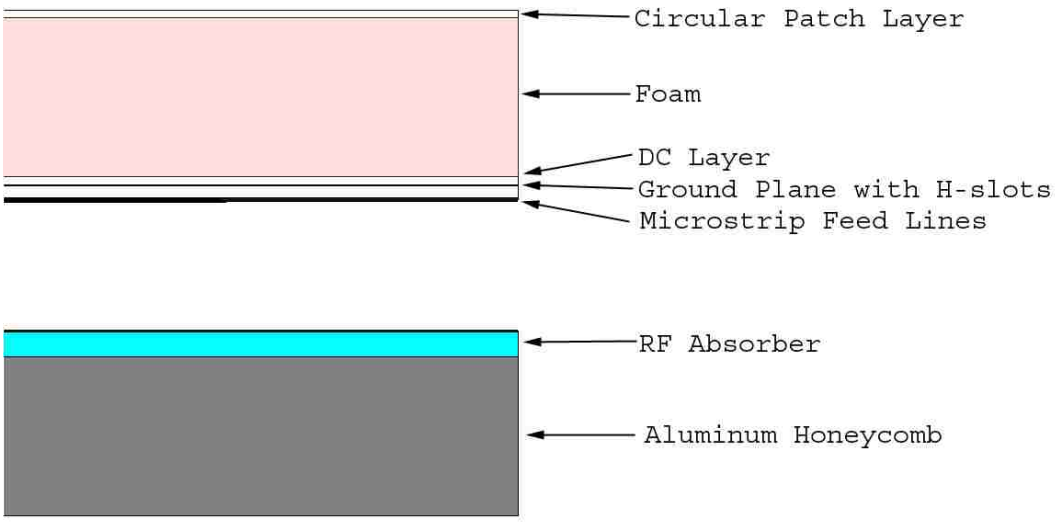

Figure 10: Detailed view of the stack up of the HSDTA.

Energy is coupled from the microstrip lines through the H-slots, which are cut into the ground plane, onto the patch. With the H-slot placed orthogonal to each other, they excite orthogonal modes on the circular patch which is turn radiates two orthogonal linear polarizations. If one introduces a ± 90° phase shift between the orthogonal slots feed lines, circular polarization is present in either the RHCP (+90° phase) or LHCP (-90° phase) sense. The radial placement of the slots, along with the slot width, slot length, and the additional microstrip matching stub length are used to tune the feed and optimize the input reflection coefficient of the antenna using CST Microwave Studio.

2.3. Active Antenna components

2.3.1. Low noise amplifiers

For a receive antenna system, it is paramount to use a low noise amplifier (LNA) as close to the feed as possible in order to establish a favorable signal to noise ratio (SNR). The further away from the feed point of the antenna, the more loss and degradation of the antenna system's maximum possible G/T. Over the last two decades, extensive research and development has been conducted in the field of Gallium Arsenide (GaAs) Monolithic Microwave Integrated Circuit (MMIC) devices. The growing popularity GaAs MMICs has allowed for mass produced, low noise amplifiers to become readily available from multiple manufacturers. These compact (typically on the order of 9-25 mm^2) units are relatively low cost and enable modern antenna designers the luxury of implementing low noise amplification to antenna arrays at locations which have been hard to access in the past.

For this design, a single LNA was used for each polarization of each antenna element. The specifications for the LNA used in the HSDTA can be found below in Table 1.

	Temperature (°C)	
	25	-40
Gain (dB)	19	18
Noise Figure (dB)	0.9	0.6
Frequency Range (GHz)	2.1 - 2.9	

Table 1: LNA specifications

Since the HSDTA will be used in an airborne application, the system is designed to operate at altitude, outside of the aircraft pressure vessel, where the temperature is approximately -50°C. The lower temperature lowers the noise figure of the LNA which in turn increases the G/T of the HSDTA. The LNA which was selected for the HSDTA requires only minimal external components and draws ~95 mA at 5 VDC. The final layout of the amplifier section of the feed can be seen below in Figure 11.

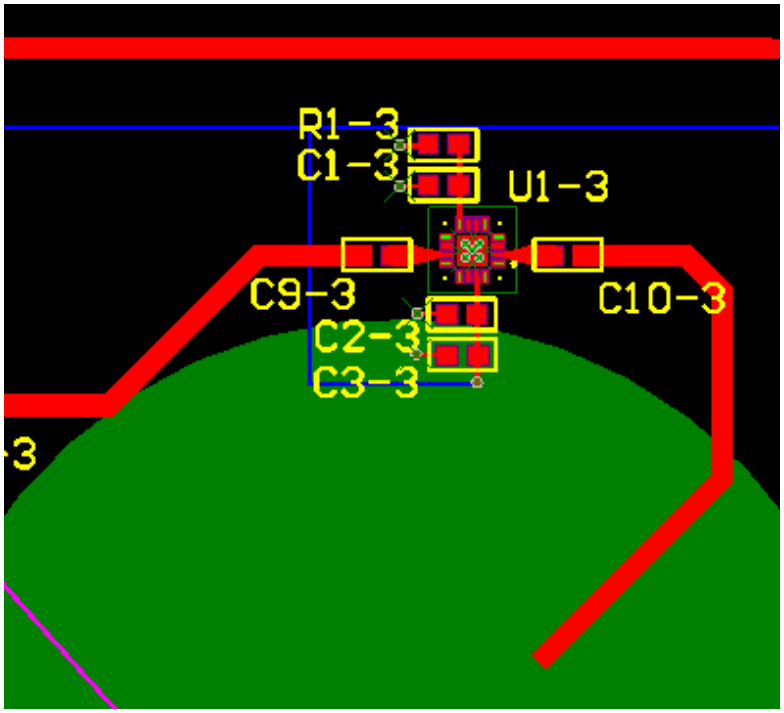

Figure 11: The LNA layout for the HSDTA

The layout of the LNA section of the HSDTA was designed to minimize the space used by each amplifier. It was critical to locate the amplifiers as close to the ACF as possible while allowing room for the feed and DC lines to be routed. DC block capacitors (C9, C10) were used to prevent DC on the RF lines while power decoupling capacitors (C1, C2, C3) and a bias resistor (R1) were used to properly stabilize the amplifier and provide the correct amount of current for proper operation.

2.3.2. Auto-tracking network

An antenna system which is capable of dynamically adjusting azimuth (AZ) and elevation (EL) pointing based on the movement of a signal source in the farfield is consider to be auto-tracking. The ability to maintaining proper pointing information for the Antenna Control Unit (ACU) regardless of the target deviating from the expected trajectory, errors in track files, or the lack of a track file is highly desirable in the telemetry field. Different configurations of auto-tracking systems include conical scan, mono-pulse, and electronic scan [12]. The conical scan configuration is primarily used with large reflector antennas and is not directly applicable to this design; therefore, it will not be discussed. To auto-track with mono-pulse and electronically scanned tracking, in both elevation and azimuth, the antenna must consist of four separate antennas which are placed in quadrants. An easy way to implement this with an array is to section the overall array into quadrants and provide a single RF output for each section which is isolation from the other quadrants.

With a mono-pulse system, a mono-pulse comparator adds each quadrant in sum (Σ) and difference (Δ) and generators an overall Σ channel, ΔAZ channel, and ΔEL channel (See Figure 12). The outputs of the mono-pulse comparator are then fed to a mono-pulse scan converter which

effectively modulates the difference channels onto the sum channel. This modulated channel can then be used by a tracking receiver to generate pointing data for the ACU.

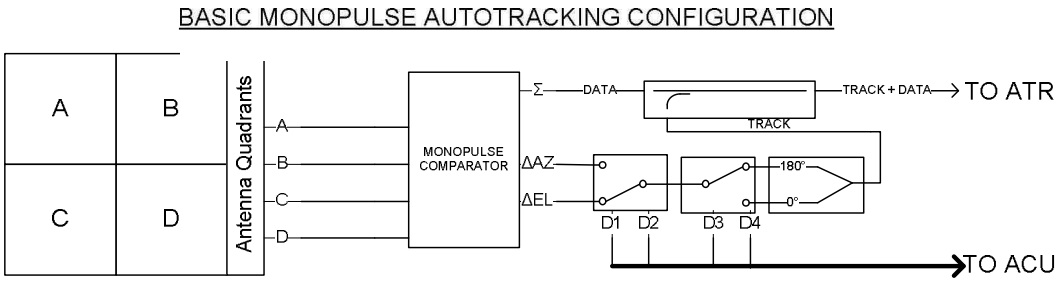

Figure 12: Mono-pulse tracking configuration.

An electronically scanned system is similar to a mono-pulse system. Four quadrants are used to generate a modulated channel which contains a sum channel, and difference channels which can be used to point the antenna. By rapidly switching between each quadrant and applying proper phase shifting, the output of an electronically scanned system is that of a mono-pulse system (See Figure 13).

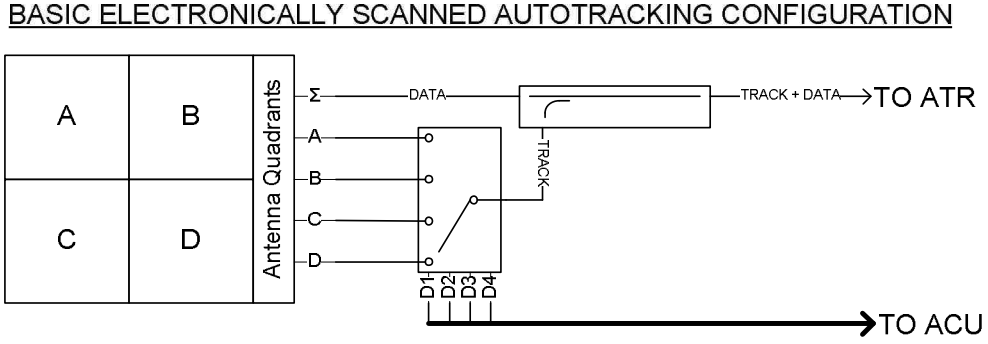

Figure 13: Electronically scanned tracking configuration.

Electronically scanned auto-tracking was selected for the HSDTA. It uses less components than mono-pulse tracking and was easily implemented on the HSDTA.

2.4. Array Design

2.4.1. Basic Array Theory

An antenna array is defined as a set of individual radiating elements which are used together to acquire a desired radiation pattern. While there are many different types of arrays, such as: linear, planar, circular, etc…, this section will discuss planar broadside arrays. A broadside array has a maximum radiation pattern normal to the plane in which the array is defined. When solving for the power pattern of an array, one must perform pattern multiplication as defined below:

$$\vec{E}(Total) = \vec{E}(\text{single element of array}) \bullet (\text{ArrayFactor}) \tag{7}$$

Therefore, in order to determine the electric fields of the overall array, one must know both the Array Factor (AF) and the single array element electric fields. For a planar rectangular array the array factor is defined by [8]:

$$AF_n(\theta,\phi) = \left\{ \frac{1}{M} \frac{\sin\left(\frac{M}{2}\varphi_x\right)}{\sin\left(\frac{\varphi_x}{2}\right)} \right\} \left\{ \frac{1}{N} \frac{\sin\left(\frac{N}{2}\varphi_y\right)}{\sin\left(\frac{\varphi_y}{2}\right)} \right\} \tag{8}$$

Where:

$$\varphi_x = kd_x \sin(\theta)\cos(\phi) + \beta_x$$
$$\varphi_y = kd_y \sin(\theta)\sin(\phi) + \beta_y$$

M	=	*x-axis number of elements*
N	=	*y-axis number of elements*
d_x	=	*x-axis element separation*
d_y	=	*y-axis element separation*
β_x	=	x-axis progressive phase shift

β_y = y-axis progressive phase shift

For broadside radiation, the progressive phase shifts should be:

$$\beta_x = \beta_y = 0$$

Also, in order to limit the number of maxima to one or two [8],

$$d_{MAX} < \lambda$$

Using these parameters, one may design a broadside rectangular array with desirable radiation characteristics; however, now it is required to have a network of power dividers in order to supply equal amplitude and phase energy to the individual antenna elements.

2.4.2. Array Feed network

Designing a feed for an array of dual polarized antenna elements, while maintaining high levels of efficiency and isolation, is not a trivial task. For broadside radiation characteristics, the splitters used in the feed network were required to be equal phase and equal amplitude. The feed network was required to fit in a single plane behind the antenna array. An additional constraint on the feed network was that the DC biasing circuitry and the low noise amplifiers are located as close to the ACF as possible.

The most common method of feeding an aperture coupled array is to design a cascade of microstrip T-junction splitters for each pair of antenna elements. The T-junction splitters use quarter-wave transformers to match the parallel impedance of the two output legs of the divider with the input 50 Ω line (See Figure 14).

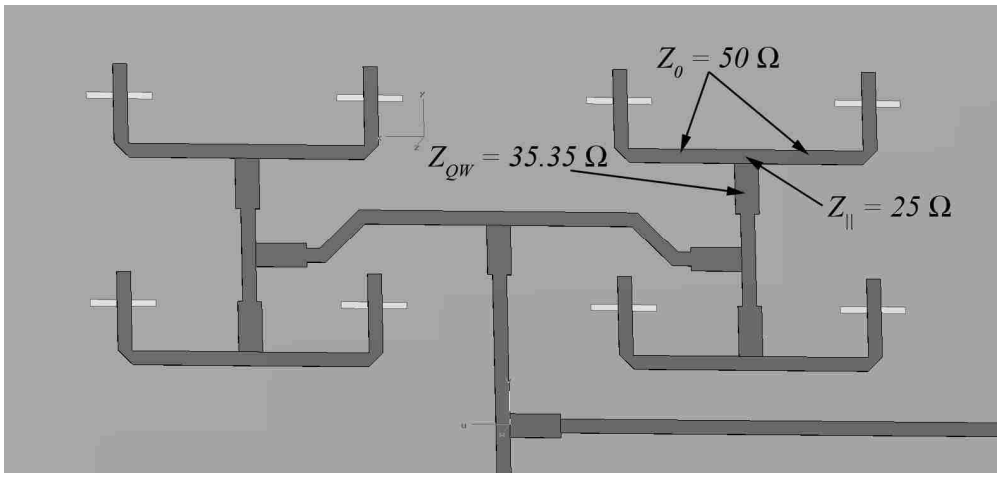

Figure 14: Example of a microstrip T-junction power divider design.

The required impedance of the quarter-wave transformer was found by:

$$Z_{QW} = \sqrt{Z_{||} * Z_{in}} \tag{9}$$

While this type of feed network was initially investigated, the relatively low frequency of operation and the implementation of dual polarization (which effectively doubles the number of elements), made the T-junction microstrip splitter not practical. Another method of power division for an array is to use discrete components.

Discrete components main advantage compared to microstrip T-junction splitters is size. At S-band, the quarter-wavelength is ~ 3.26 cm. With these dimensions it is challenging to fit a single polarization on the back of an antenna let alone two polarizations. The main disadvantage of discrete components is insertion loss. For this design, the added insertion loss is not a significant problem provided the LNAs have sufficient gain.

The final HSDTA feed network design uses a cascade of two way power combiners to first combine a single antenna pair, then combine two antenna pairs. After a row of four elements is combined, the additional

combination of the elements is taken through a surface mount SMA connector to external power combiners which are located on the rear of the aluminum honeycomb. Having the first two stages of power combination on the actual circuit boards saves significant amounts of money, time and removes the added complexity of connecting 32 SMAs to each antenna tile. Feeding the HSDTA this way proved to be ideal for a dual polarized antenna system. The different feed points of each antenna element could all run parallel to the center of the antenna tile and then be taken off the board for additional combination and to feed the auto-tracking circuitry as can be seen in Figure 15.

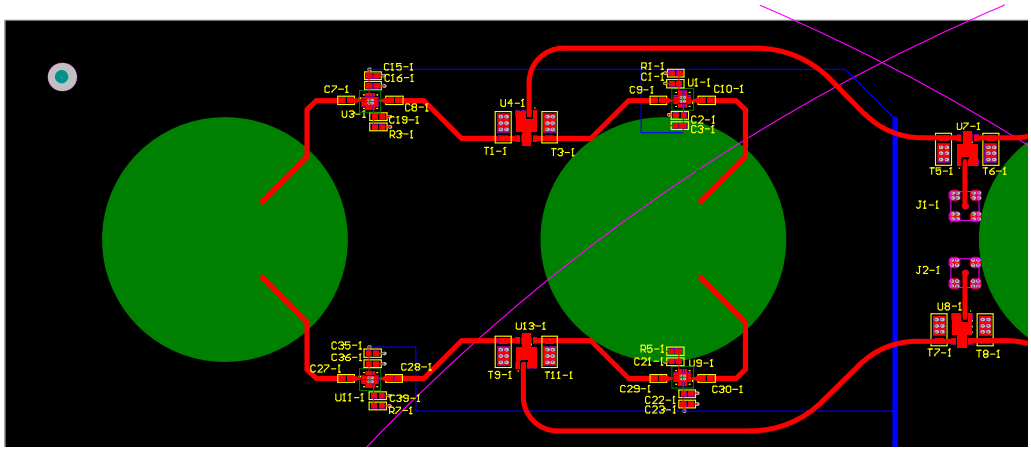

Figure 15: Single element pair final feed network including the SMA connector.

The layout of the feed lines, power combiners, and LNAs as can be seen above in Figure 15 was done using a commercial PCB layout code, Altium Designer. In order to provide sufficient isolation between the feed lines, care was taken to separate each line by a minimum of three times the width of the microstrip. This distance was chosen to allow the electric and magnetic fields between the ground plane and the microstrip line sufficient distance to decay significantly. The DC layer of the board, as indicated by the blue traces, is used to provide power and proper biasing to the LNAs. As can be seen in Figure 10, the DC layer was placed on the opposite side of the microstrip feed layer separated by the ground plane. Care was also taken to locate the DC lines as far away from the H-slots of the ACF

to minimize the interaction between the DC and RF performance of the HSDTA.

A complete quadrant of the HSDTA can be seen below in Figure 16. Note the eight SMA connectors running down the center of the tile which carry the RF signals and the BNC connector located at the center of the antenna tile which provides the DC power for the active components of the tile. The violet curves seen on the tile are placed there for reference showing where each tile could possibly be cut to build a 34" antenna.

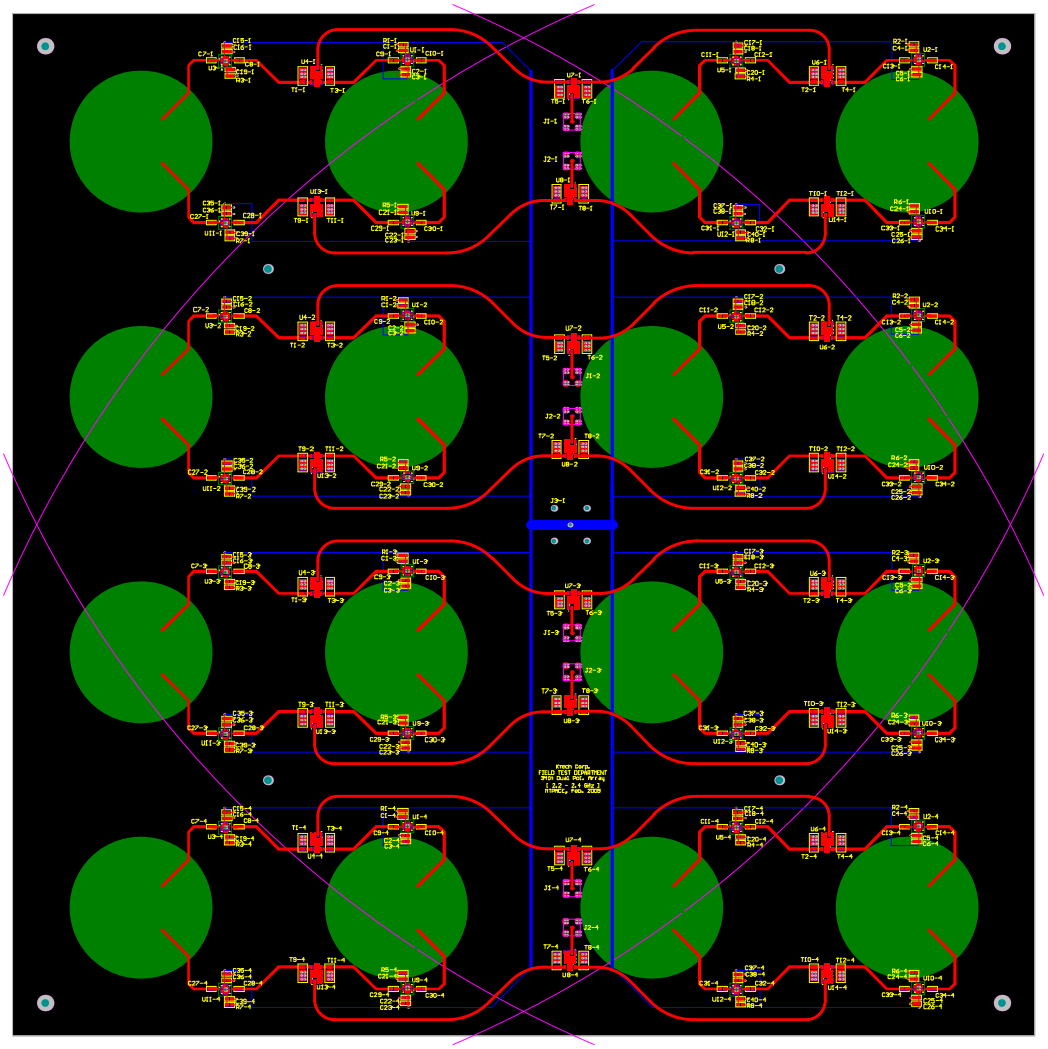

Figure 16: A complete quadrant of the HSDTA. Note the violet curves showing possible cut points to for each quadrant.

2.4.3. Final Array Design

The final array was designed to be resonate at 2.3 GHz. The maximum radiation pattern was desired to be broadside with an E-Plane half power beam width (HPBW) on the order of 10 degrees and an H-plane HPBW on the order of 10 degrees. The gain of the antenna was designed to be 25 dBi. To meet these requirements while remaining within the size restraints, the number of elements was determined to be: M = 16 and N = 16.

The X and Y spacing between the patch elements was chosen to be approximately 0.7 λ_g. This was chosen as a compromise between the optimum spacing for broadside radiation (~0.5 λ_g) and the ability to physically fit the entire feed network compactly behind the patches. The actual dimensions of the array can be found below in Table 2.

An important constraint on the design of the antenna system was that it was flexible enough to be physically resized to fit in a variety of different aircraft radomes. The most cost effective solution to this problem was to make a base antenna tile which is comprised of a 4x4 antenna array. The base antenna tile was then placed into quadrants to expand the size of the array to 16x16. Each of the antenna tiles was fed separately so that quadrant based electronically scanned auto tracking could be implemented (See Figure 17).

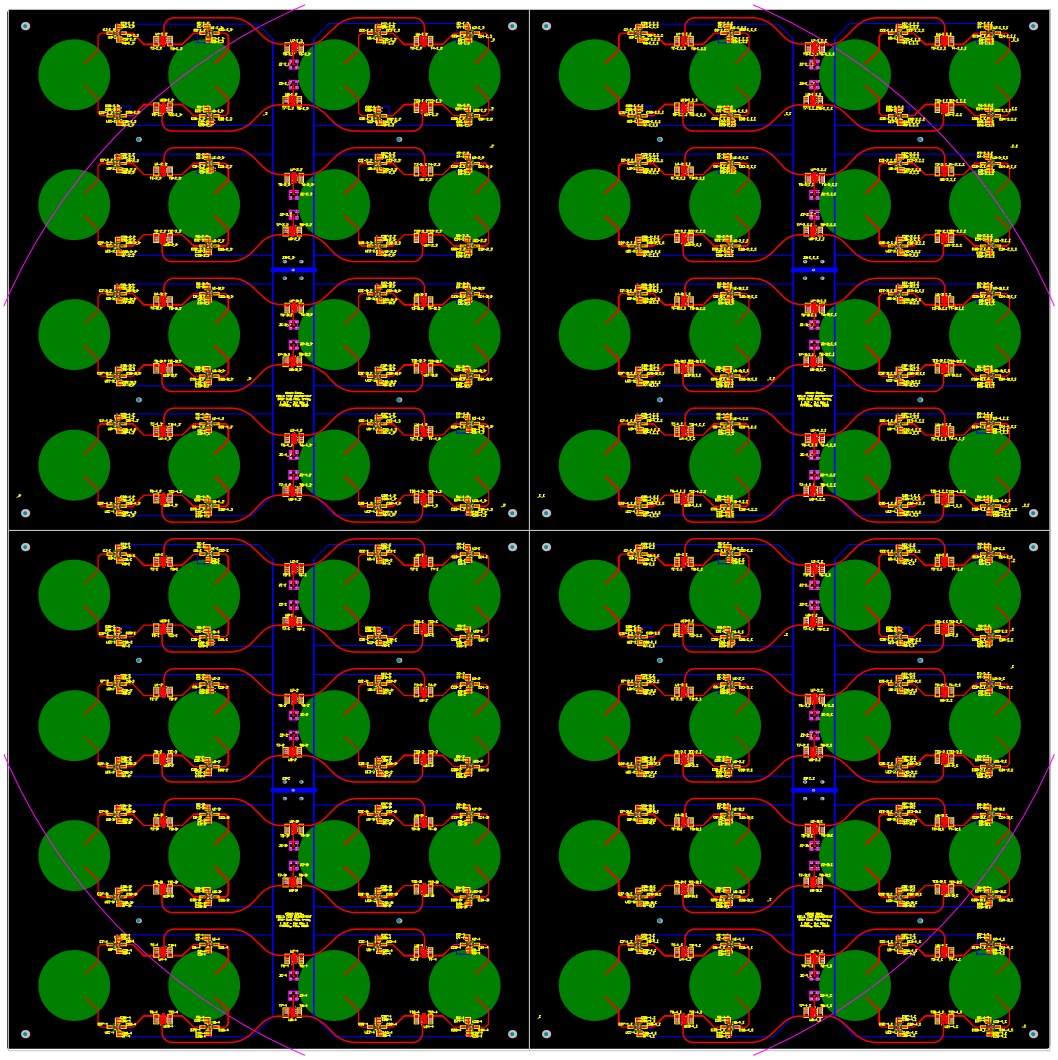

Figure 17: Full modeled array. Note the violet curves denoting a 34" diameter circle

The HSDTA was designed to go on a variety of airborne assets each with different radome shapes and mounting locations. By designing an antenna system that can be used on multiple assets, overall program risks decrease along with significant cost savings. The HSDTA will be physically rotated by a pedestal from +90° to -90° in azimuth and -10° to +90° in elevation. Without changing the thickness of the array, the main dimension constraining movement is the diameter.

A single HSDTA can be permanently cut into different diameters as can be seen in Figure 18. Elements of the HSDTA are lost as the diameter of the array is decreased; however, apart from the inherent reduction in gain, the

performance of the array remains comparable between different diameters. This was accomplished by properly terminating the inputs of the power dividers which are not in use due to the decreased number of elements. This also allows for only one base antenna design to be qualified for flight.

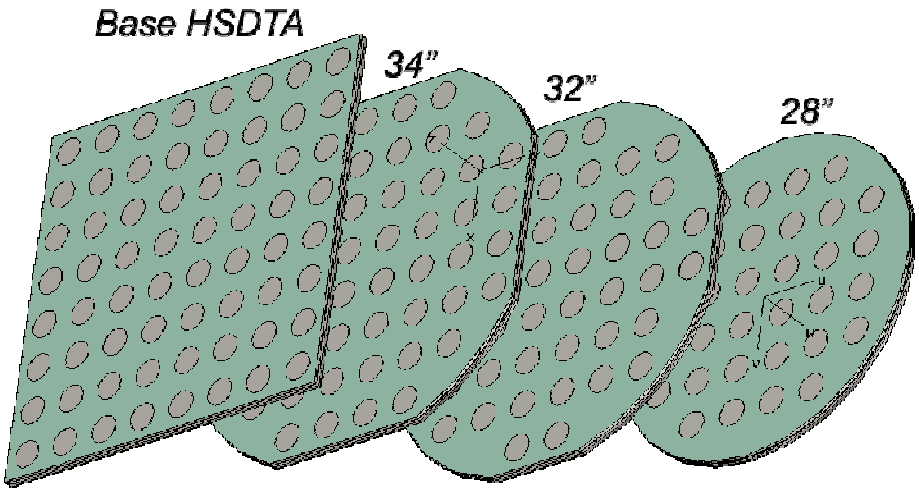

Figure 18: Model of multiple cut HSDTAs.

At each of the inputs of the power dividers, an unpopulated pad was placed where a RF termination could be populated if needed (Figure 19). The terminations are required to maintain the amplitude and phase balance of the feed network. This system proved to be a cost effective method of using a single base antenna tile for multiple aircraft, while maintaining high levels of efficiency for each asset.

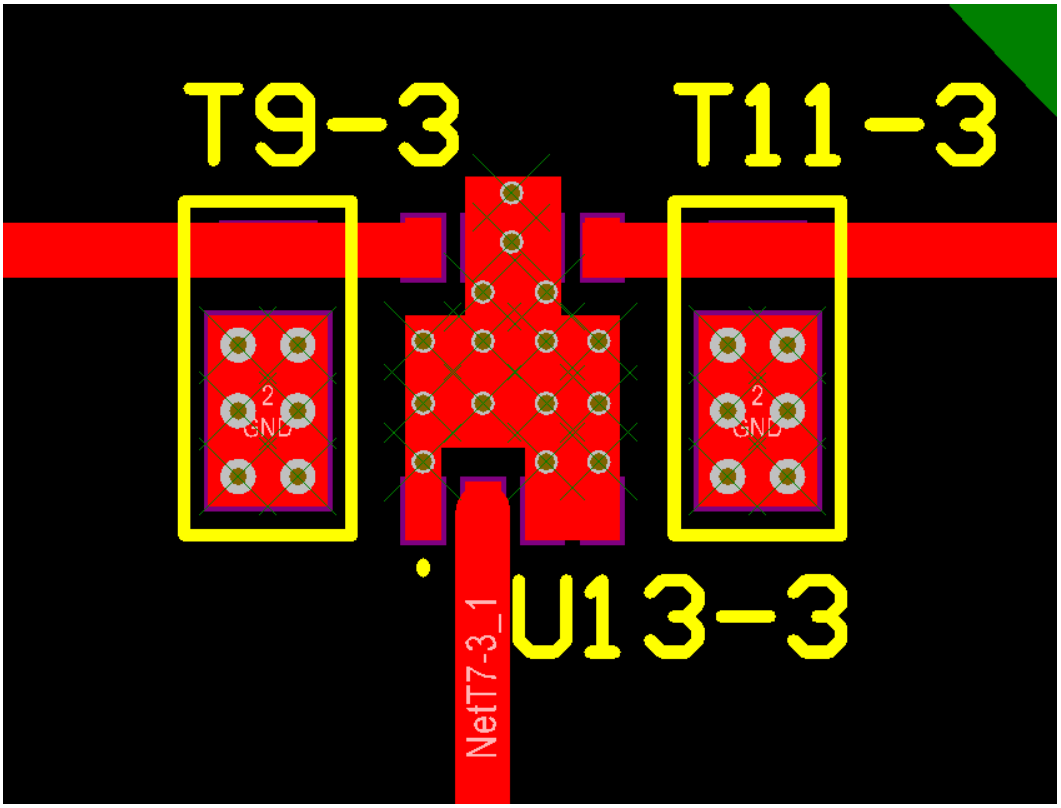

Figure 19: Layout of power dividers to provide termination for the multiple configurations of the HSDTA.

2.5. Simulation

The design of the HSDTA was completed in CST Microwave Studio. The goal of the simulation was to obtain a parameterized model of the entire array which could be optimized for a specific band of interest. The simulation was used to validate the design of the circular patch, the feed network, and the composite material stack-up of the HSDTA. Due to symmetries in the feed network, the base element for the HSDTA was a pair of two patches (See Figure 20).

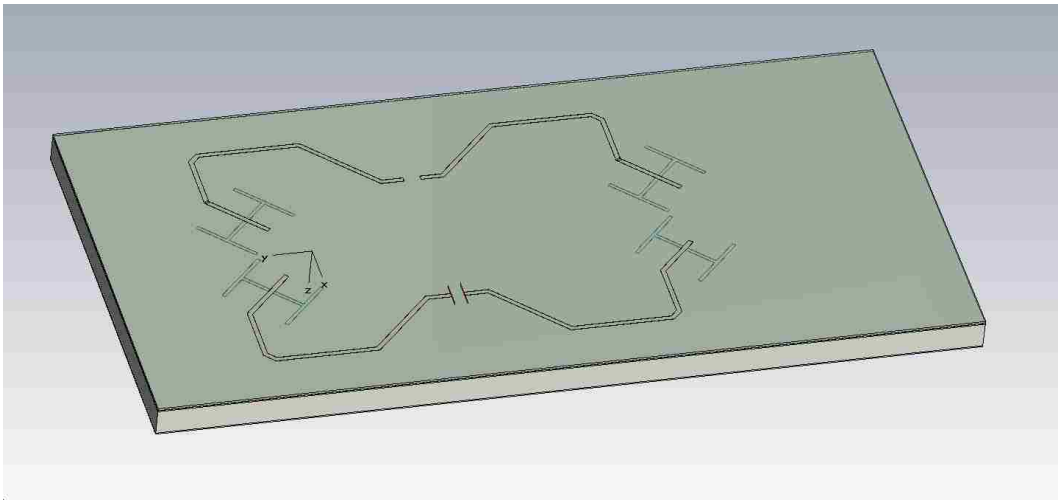

Figure 20: Model of the base antenna element pair.

Since dual circular polarization was an important design goal for the HSDTA, the farfield electric fields generated by the feed network and the patch were analyzed to determine polarization purity and sense based on different input phasing conditions. The electric field from the two orthogonal feeds can be seen below in Figure 21.

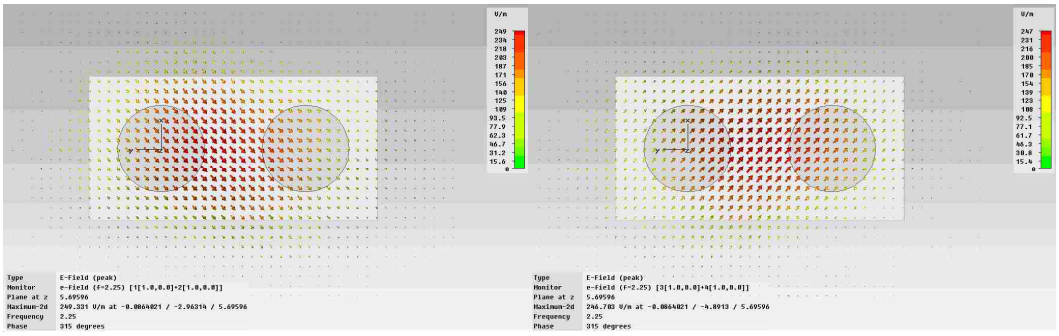

Figure 21: The electric field from both linear polarized ports to the circular patch.

The initial simulation of the base element pair did not include the LNAs or discrete power dividers. By placing these components after the electromagnetic simulation was completed, the model was greatly simplified. This model works assuming the input impedance to the array is

real, and equal to 50 Ω. The parameters which relate directly with the center frequency of the HSDTA are: the patch radius, X and Y array spacing, and microstrip line width. With these parameters defined, the arrays input impedance bandwidth had to be optimized. The primary parameters which affect the impedance bandwidth of the array are: the height of the substrate, dimensions of the H-Slot, and the length of the matching stub associated with each slot. These parameters were optimized in CST Microwave Studio to produce acceptable S11 performance.

Once the base antenna element pair was optimized for the band of interest (2.2 – 2.4 GHz), it was used to form a quadrant of the overall array. This quadrant was then simulated to ensure that mutual coupling would not adversely affect the performance of the HSDTA. The final model of a quadrant of the array can be seen below in Figures 22 and 23.

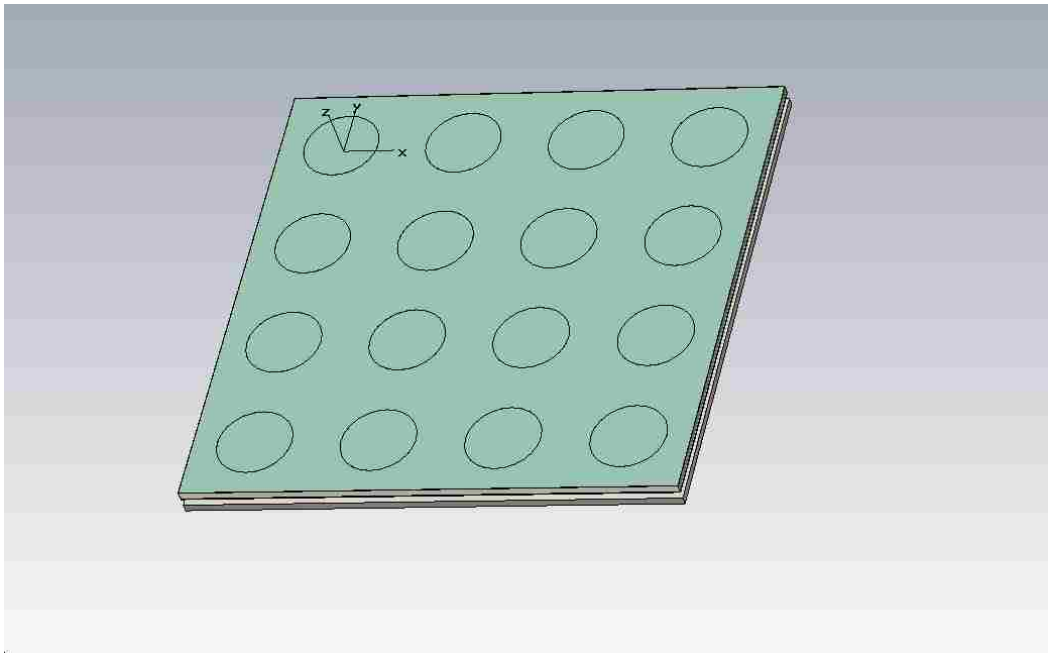

Figure 22: Front side of fully modeled array.

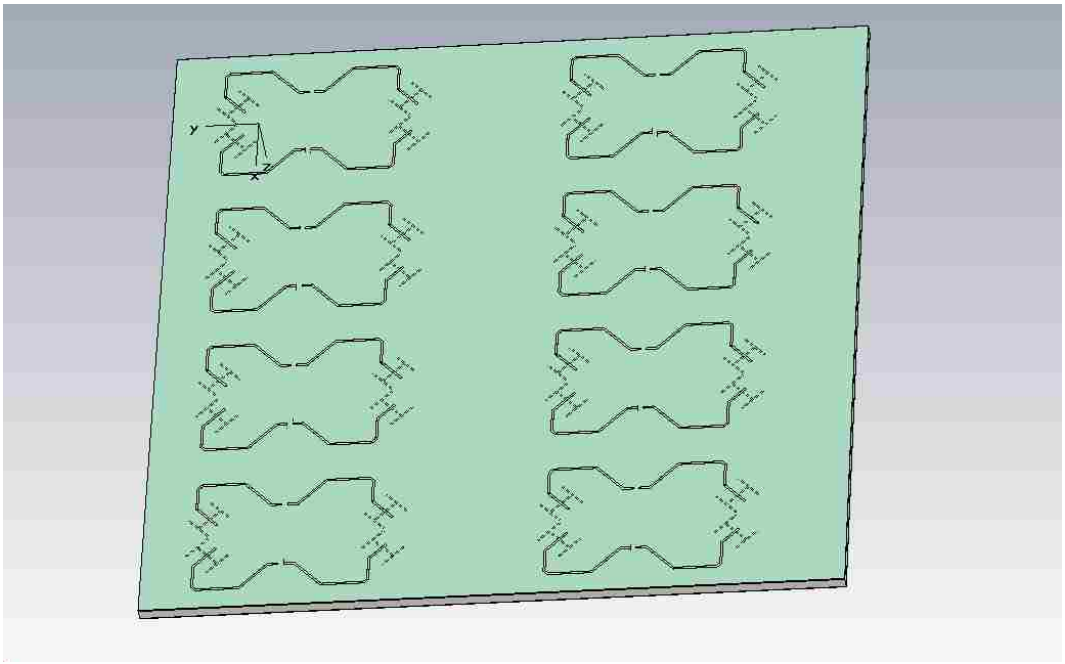

Figure 23: Back side of fully modeled array.

Once, a quadrant of the array was completely simulated in CST MWS, the finished model was transferred to PCB layout software where the remaining components were added along with connectors and mounting holes. The final parameters used to fabricate a prototype antenna array are summarized in Table 2:

Patch Antenna:		
a	2.958	cm
h	0.6654	cm
Aperture Coupled Feed:		
Microstrip width	0.1138	cm
Microstrip substrate thickness	0.0508	cm
Array Quadrant		
d_x	9.782	cm
d_y	9.782	cm
M	4	
N	4	
Overall X Length	41.91	cm
Overall Y Length:	41.91	cm
Overall Thickness	2.020	cm

Table 2: The final parameters of the simulated array.

2.6. Fabrication

The substrate material used to fabricate the array is a glass woven fiber based substrate which is easier to manufacture than Teflon based substrates. The characteristics of the material are summarized below in Table 3. The data shown in Table 3, was provided by the manufacturer of the material at a frequency of 10 GHz. The material properties are sufficiently frequency independent for use on the HSDTA which operates from 2.2 to 2.4 GHz. Using a glass woven fiber based substrate helped to lessen the cost and lead time of the final array. The RF input ports to the array are surface mount SMA connectors. The final assembled base antenna quadrant tile can be seen below is Figures 24 and 25.

Substrate Material Characteristics	
Dielectric Constant, ε_r	3.38
Dissipation Factor, tanδ	0.0027
@ 10 GHz / 23°C	

Table 3: Properties of the substrate material.

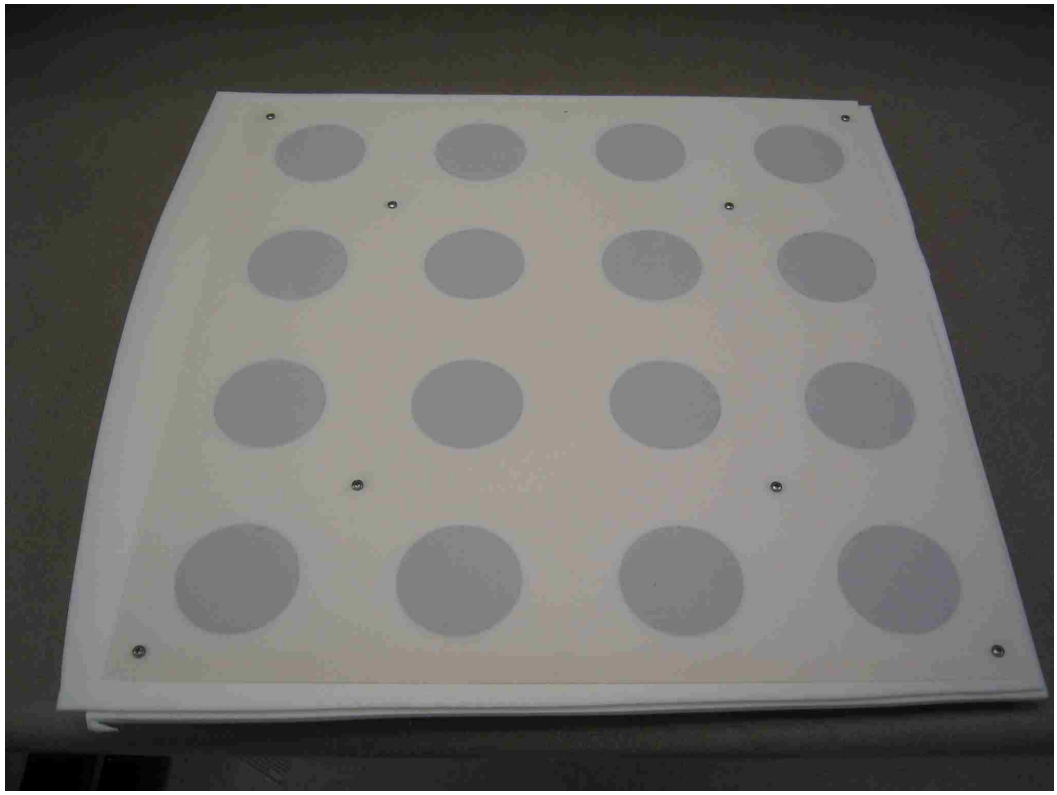

Figure 24: Front side of the base antenna tile.

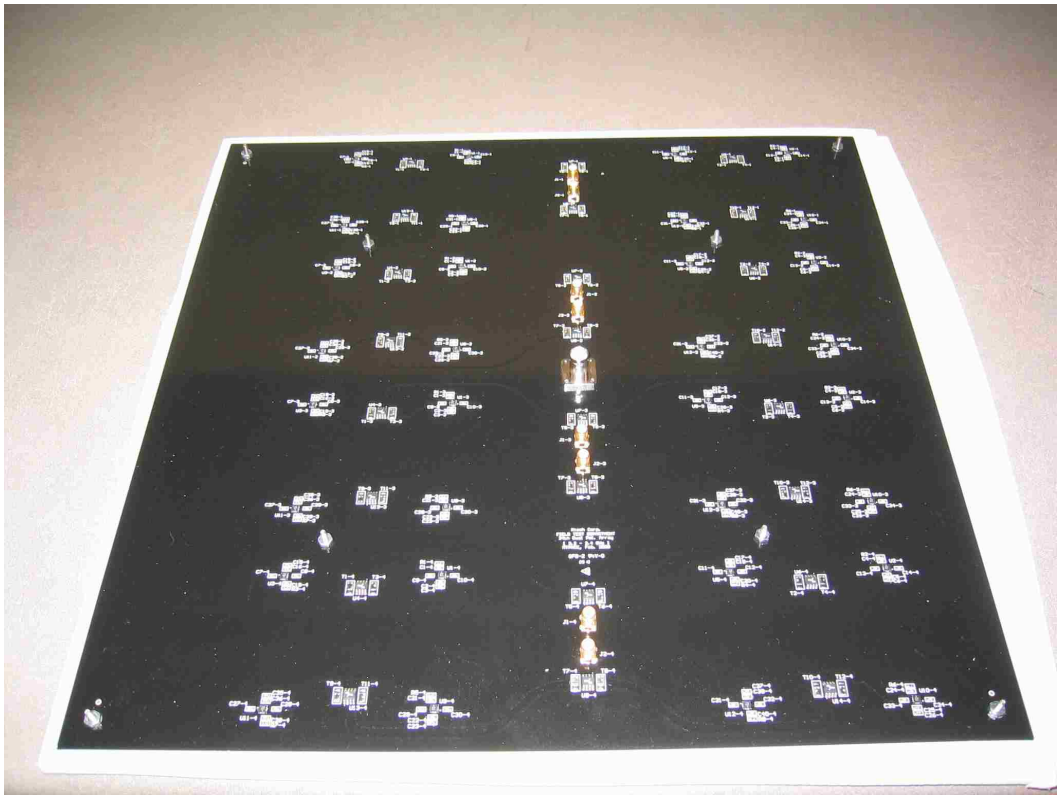

Figure 25: Back side of the base antenna tile.

After the base antenna tiles were populated with the passive and active RF components, each tile was sent through a conformal coat process to protect the active components from condensing liquids while flying. Next, each tile was cut to form a 34” diameter quadrant and was assembled on the aluminum honeycomb base plate which was coated with RF absorber. Finally, the external components for auto-tracking and quadrant combining were installed on the back side of the aluminum honeycomb. The final assembled antenna system can be seen below in Figures 26 and 27.

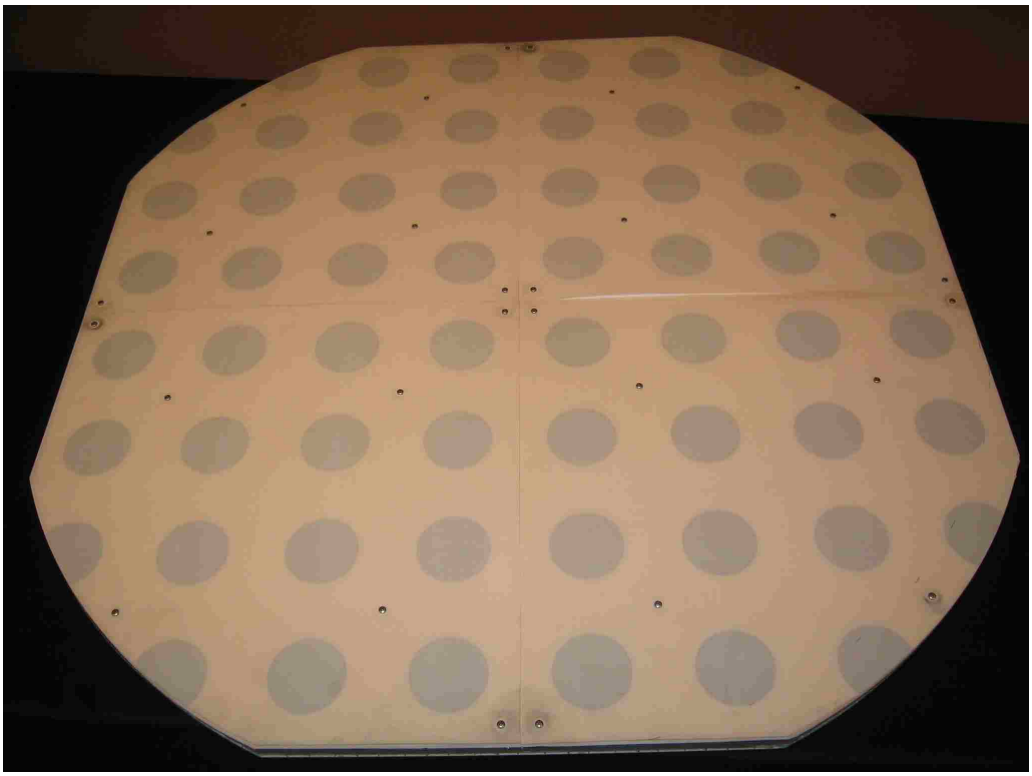

Figure 26: Front side of the fabricated and cut 34" HSDTA.

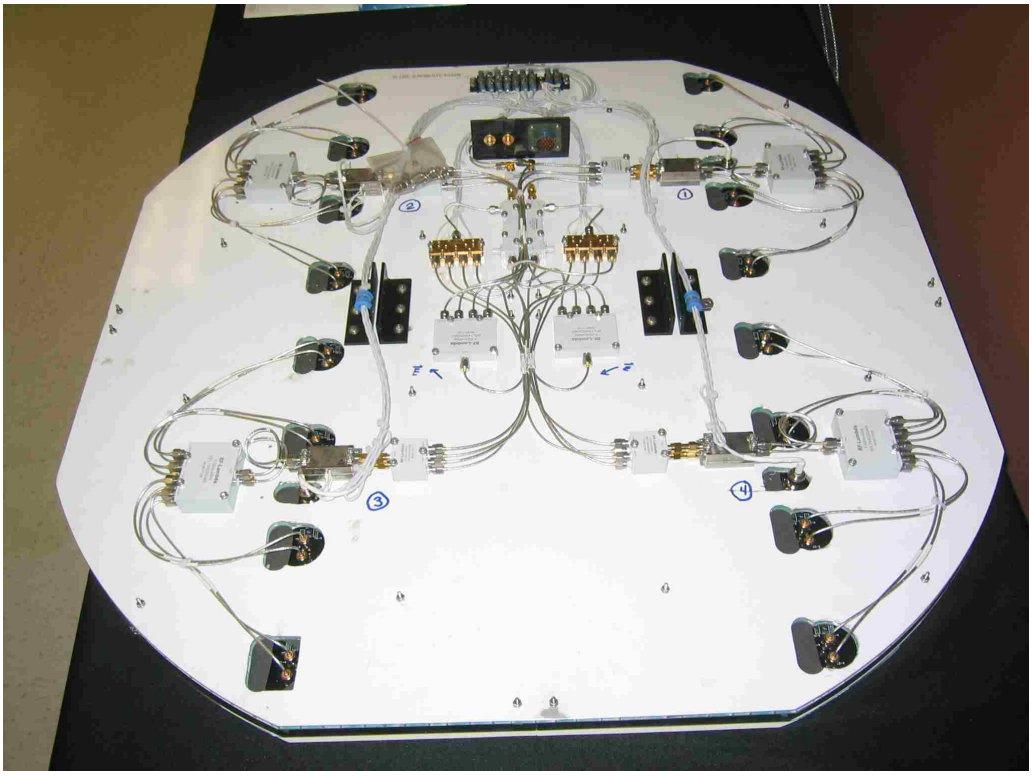

Figure 27: Back side of the fabricated and cut 34" HSDTA, note the auto-tracking components mounted on the aluminum honeycomb structure.

CHAPTER 3

Results

After the HSDTA was simulated and fabricated, it was tested at Ktech Corporation's outdoor antenna range. Using a HP 8753D vector network analyzer, the HSDTA was swept in frequency to verify the input reflection coefficient. Next, the HSDTA was placed on Ktech's airborne pedestal and the radiation pattern was recorded in both the E and H-planes. Using a set of standard gain horns, the gain versus frequency was measure followed by a measurement of the system noise temperature of the HSDTA. Finally, the antenna G/T was calculated. The G/T was further verified through a successful mission deployment of the HSDTA where the system collected telemetry of a launch event while flying on an airborne asset at 35000 ft. The receiver power levels and data quality from the mission were in close concordance with simulated values.

3.1. DC Operation Verification

Each antenna tile was tested to verify the basic operation of the LNAs. As a first order test, the LNAs were verified to be pulling the correct amount of current. The overall current draw for each antenna tile was recorded and compared as can be seen below in Table 4. With 26 amplifiers per tile, each drawing around 30 mA, the results shown prove to be valid.

Antenna Tiles Power Draw	
Quadrant	Current (mA)
1	760
2	751
3	760
4	780
Voltage: 5.09 V	

Table 4: Antenna tile current draw.

As an additional verification that each LNA was working correctly, a thermal image of each quadrant was taken. The heat signature produced by a correctly operating LNA was used to verify proper operation of the quadrant as can be seen below in Figure 28.

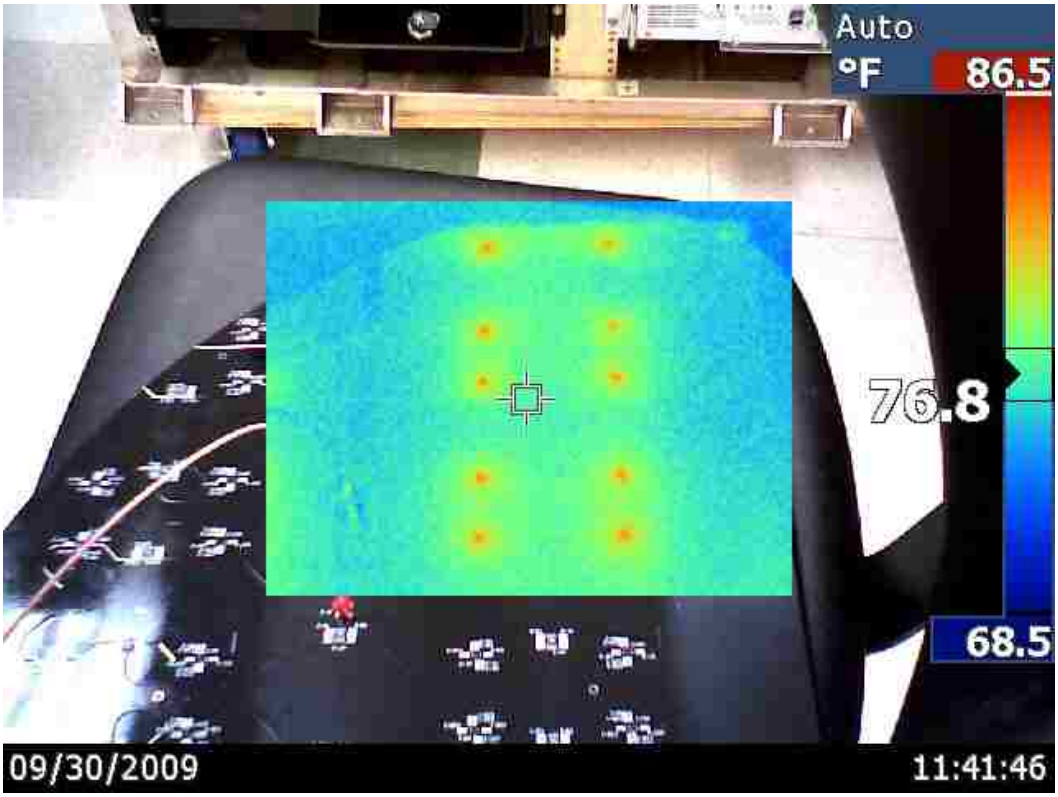

Figure 28: Thermal image showing the heat signature of the LNAs during correct operation.

In the case where an LNA is non-operational, either due to infant mortality or improper processing and handling, the heat signature would not be present on the thermal imagery. From the eight antenna tile boards which were order, only one LNA on a single tile was not operation as can be seen below in Figure 29.

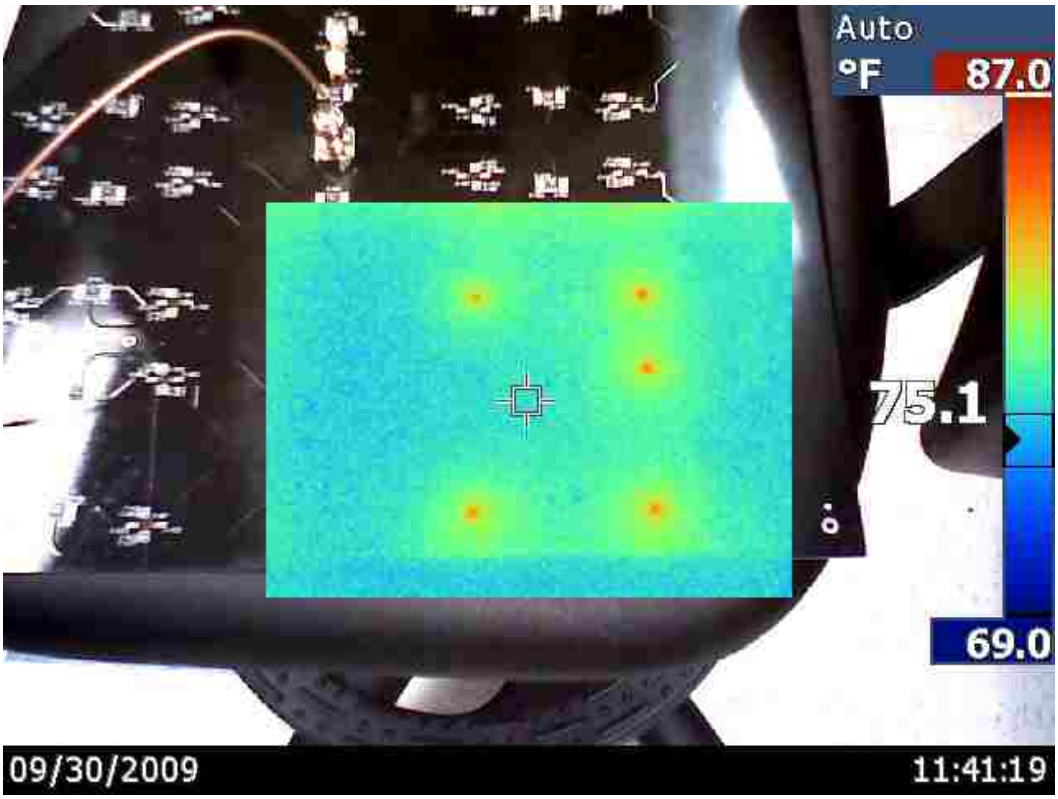

Figure 29: Thermal image showing an LNA which was not functioning correctly.

The combination of thermal imagery and current draw measurements verifies the DC performance of the LNAs along with establishing the bias operating current of each device. While the bias current is useful in determining the basic RF performance of each amplifier (from the provided datasheet of the LNA), it is not a validation that the RF portion of the LNAs is working properly. In order to measure the RF performance of the HSDTA, each quadrant was tested using a HP 8753D network analyzer.

3.2. S-Parameters

The final simulated input reflection coefficient, or S11, of an element pair can be seen below in Figure 30. Both ports of the element pair are well matched and track each other well across the band of interest, 2.2 – 2.4 GHz.

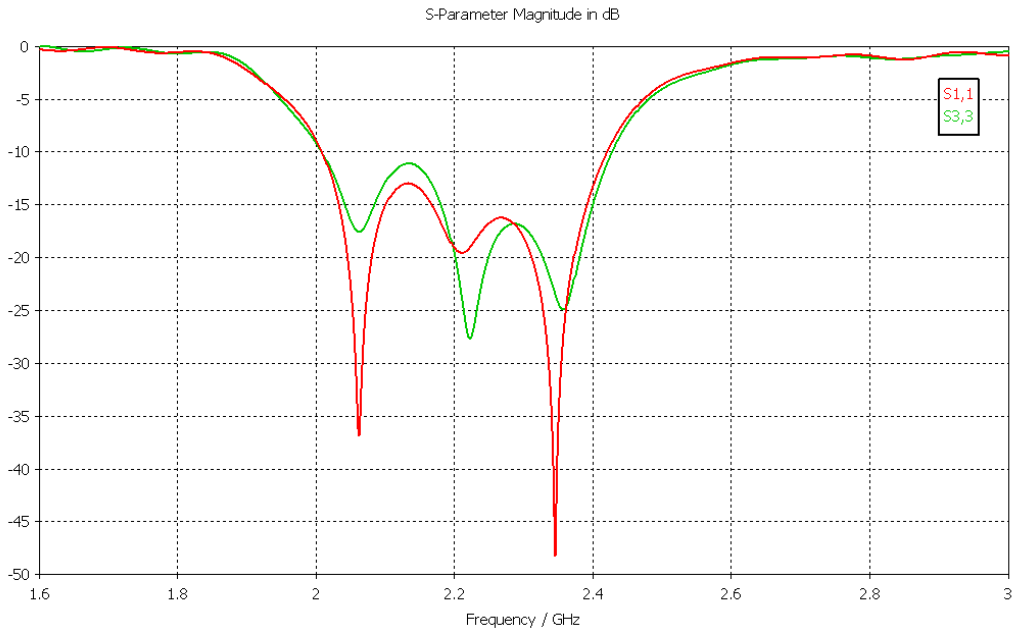

Figure 30: The simulated S11 of a base element pair.

Due to the cascade of components following each ACF, the input reflection coefficient, or S11, of the antenna could not be directly measured. The method used to determine the pass band of the antenna involves relies on a standard gain horn and a network analyzer. By setting up an outdoor antenna range and measuring the through power (S21) of the system when excited by a wideband standard gain horn, the S11 of the HSDTA can be interpolated (see Figure 31).

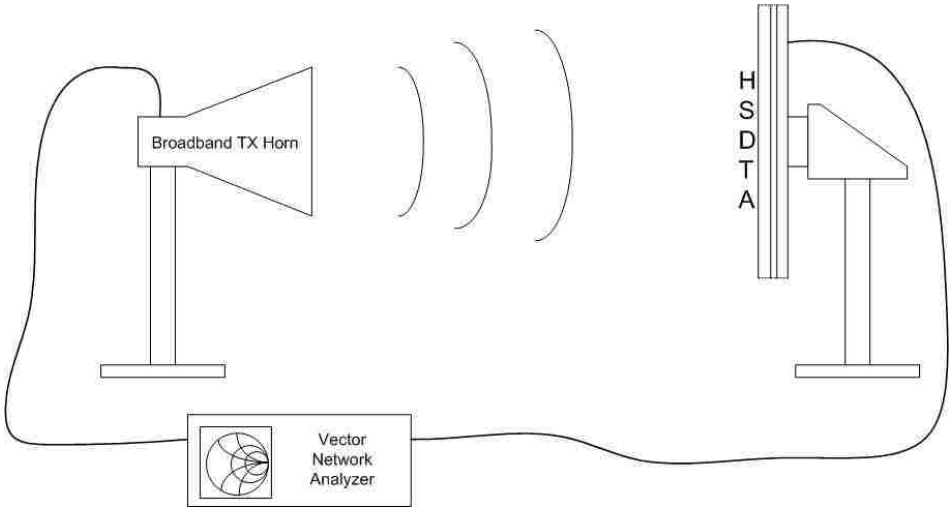

Figure 31: Antenna range setup for the S11 measurement

The power measured at the HSDTA is plotted as can be seen in Figure 32. The S21 of the system is greatest from 2.2 to 2.4 GHz which implies that the HSDTA is non-reflective and well matched across that band.

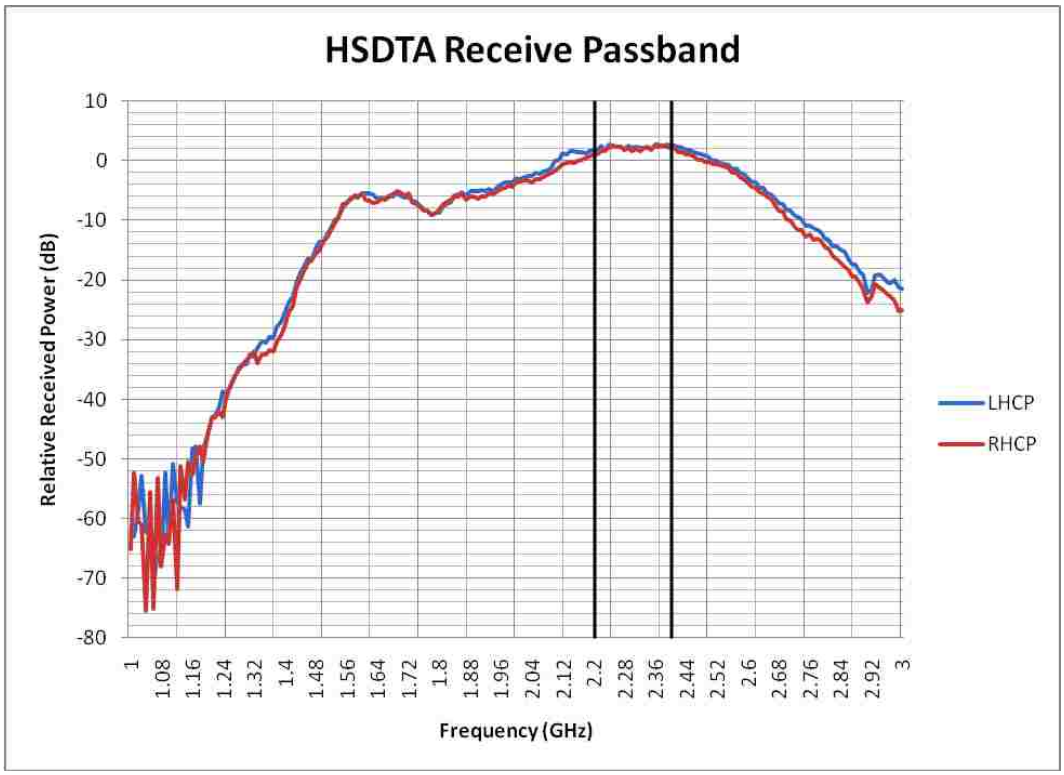

Figure 32: Measured Receive power of the HSDTA. The desired pass-band of the system is denoted by the bold lines.

3.3. Radiation Patterns

The radiation patterns of the HSDTA were measured using the Ktech Corporation's outdoor antenna range. The HSDTA was excited using a linearly polarized standard gain horn. The measured verses simulated radiation patterns were very similar (see Figure 33). The frequency of the patterns is 2.250 GHz, which corresponds to the best resonant frequency found in Section 3.2. The pertinent antenna parameters are summarized below in Table 5.

Array Radiation Pattern Characteristics			
		Measured	Simulated
E-Plane	HPBW (degrees)	10.0	10.0
	Side lobe Level (dB)	-16.3	-19.0
	Gain	23.71	25.0

Table 5: Radiation pattern measured vs. simulated results.

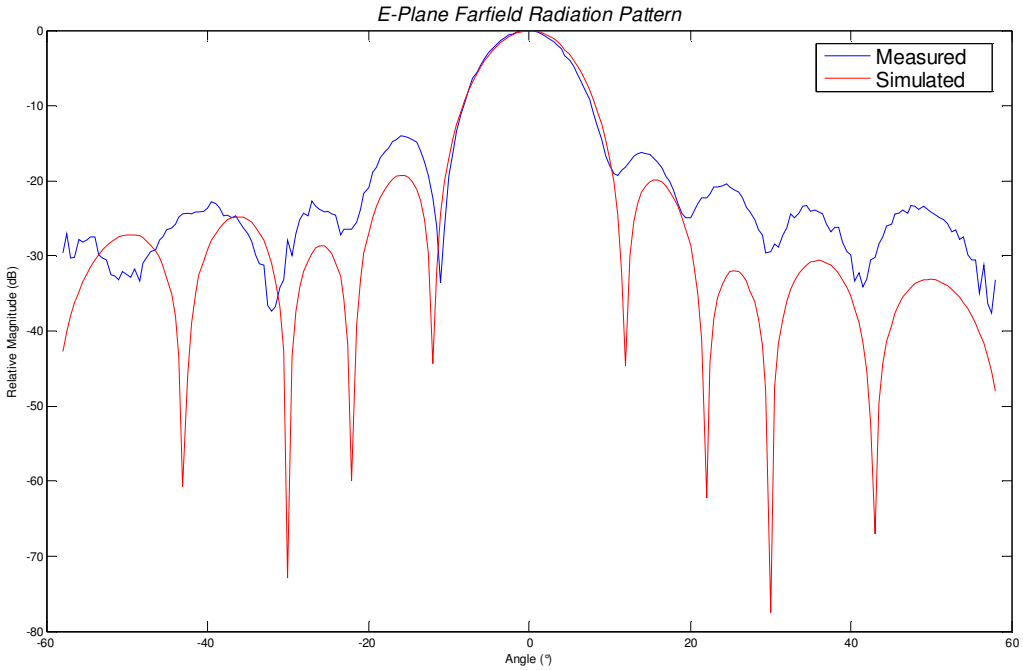

Figure 33: Simulated vs. measured E-plane radiation pattern.

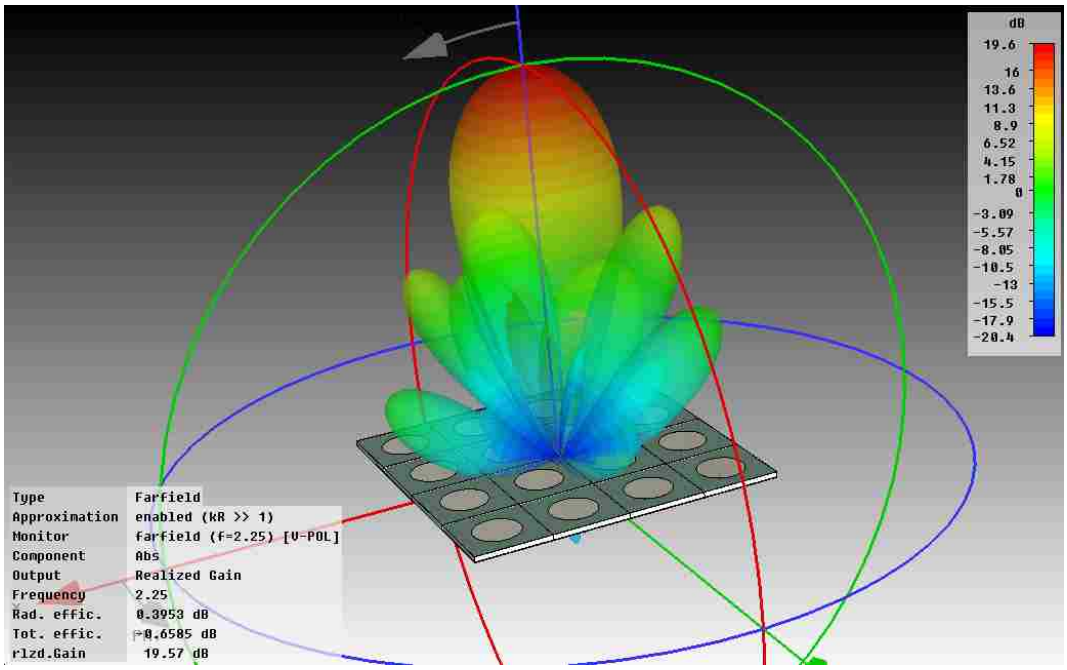

Figure 34: Simulated 3-D radiation pattern with array.

In figure 34 above, the simulated 3-D radiation pattern of a single antenna tile is shown. As expected, the radiation pattern in symmetric in the E and H-planes. The similarities in the beam width on nulls between the measured and simulated radiation pattern shown in Figure 33, verifies that each element of the array is operating correctly. The measured difference in side lobe level, while acceptable, can be contributed to the amplitude variation of each LNA and could be alleviated by implementing an amplitude distribution on the array. Overall, the results of the radiation pattern measurement were positive and validated the electromagnetic design of the HSDTA.

3.4. Antenna System Noise Temperature

The antenna system noise temperature of the array was calculated using two separate methods. The first method is typically used for larger aperture antenna whose beam widths are on the order of <5°. This method utilizes the difference in the noise floor of the system when varied between hot sky (the Sun) and cold sky. The second method has been proven [13] to work on smaller antennas; it involves using an RF absorber test fixture which is at a known temperature and cold sky.

To measure the antenna system noise temperature of a large aperture antenna, the noise spectrum of the antenna must be measured while it is pointing at a “hot” noise source, such as the sun and a “cold” noise source such as empty astronomical sky. The difference in power between these noise measurements is used along with the solar flux to calculate the system noise temperature [12]. The pointing of the antenna must be fined tuned while on hot sky to maximize the noise levels and on cold sky to minimize the noise levels [24]. For the HSDTA, the beam-width is on the order 10° which leads to a spot size with a diameter of approximately 26 million km at a range of 150 million km. For the sun, which is located approximately 1.4 million km away from the earth and has a diameter of approximately 1.4 million km, this spot size leads to inaccurate results with the HSDTA. Another method of measuring the antenna system noise temperature was explored which did not involve far off celestial objects.

The second method offers a more controlled environment where one does not rely on the daily solar flux values and precise antenna pointing towards the sun for hot sky measurements. With this method, the antenna system is placed directly under a large sheet of RF absorber and the noise

spectrum is measured on a spectrum analyzer [13][14]. Once this measurement is recorded, the RF absorber is removed and the noise spectrum is then measured again for the cold sky. Both of these power spectrums along with the associated Y-Factors can be seen below in Figure 35.

The delta power level between the absorber and the cold sky is known as the Y-factor (10). Using the temperature of the absorber and an estimate of the cold sky temperature, one may calculate the antenna system noise temperature T_s (11) [24].

$$Y_{FACTOR} = P_{ABSORBER} - P_{COLDSKY} \tag{10}$$

$$T_s = \frac{T_{HOT} - (T_{COLD} * Y_{FACTOR})}{Y_{FACTOR} - 1} \tag{11}$$

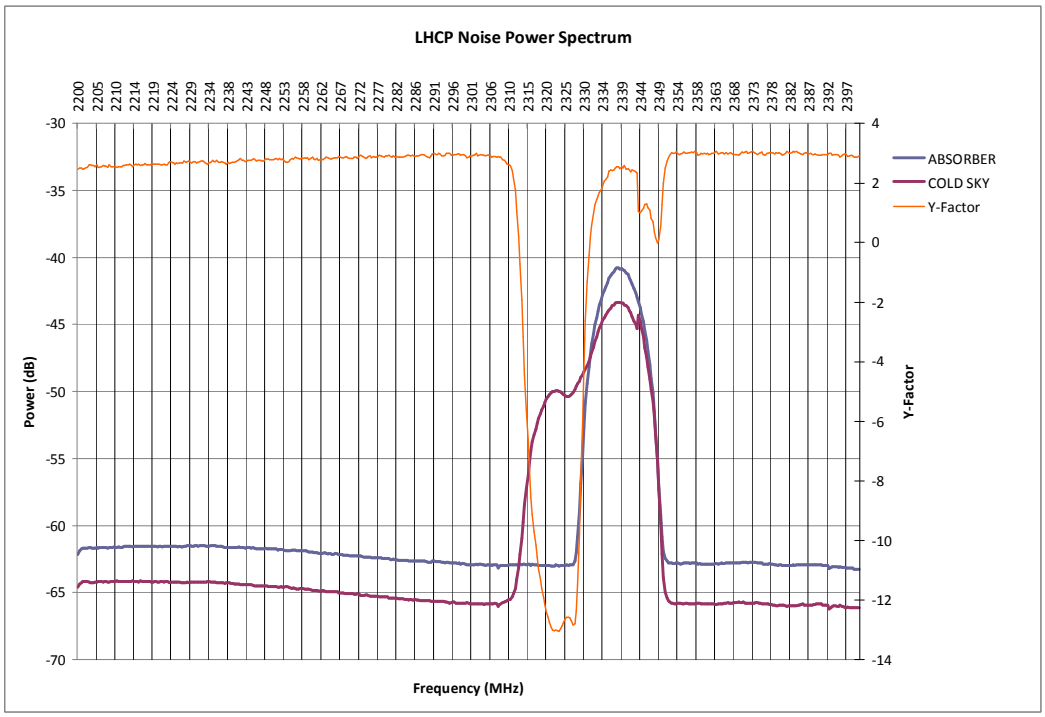

Figure 35: LHCP noise power spectrum of the HSDTA using both RF absorber and cold sky.

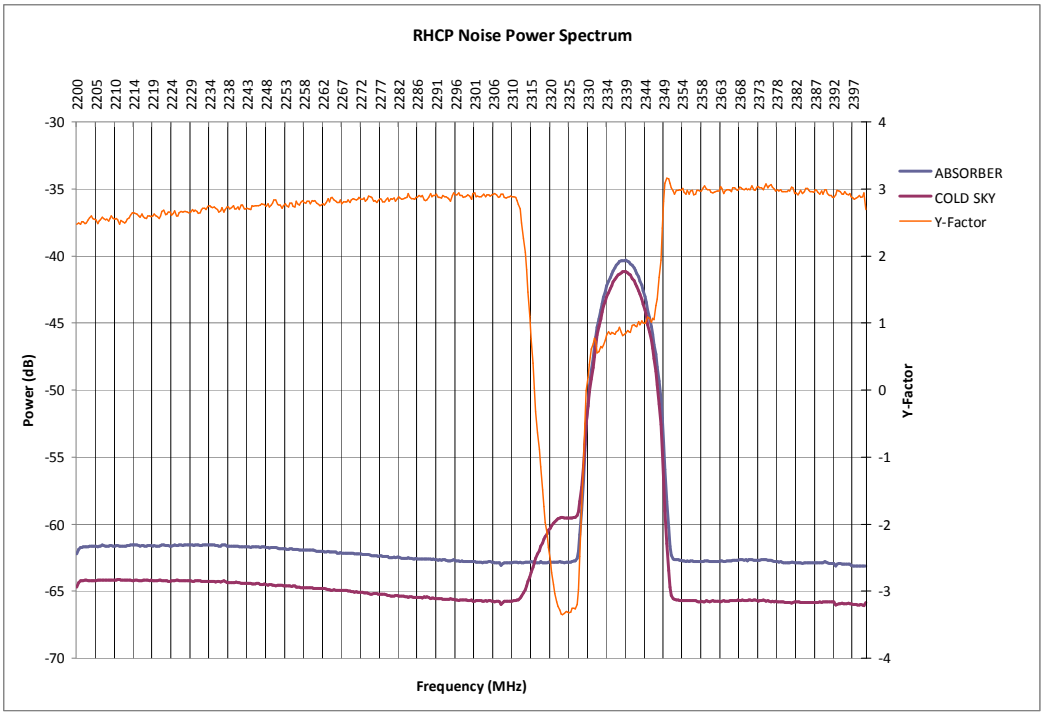

Figure 36: RHCP noise power spectrum of the HSDTA using both RF absorber and cold sky.

The spikes in the noise spectrum, which are independent of both the Cold sky and the absorber, represent local RF interference. In the LHCP case, it is interesting to see additional interference located around 2300 MHz. This spike in power is believed to be cause by XM satellite radio which is located in this band and is LHCP. The significant attenuation of this signal with the absorber shows that the test setup is functioning correctly and the noise power is really that of the absorber and not additional celestial objects. The noise power spectrum is not valid in the regions of either celestial or local RF interference; therefore, the noise power in these frequency regions is to be ignored.

From the results seen in Figure 36, the antenna system noise temperature was calculated using (11) in both LHCP and RHCP (See Figure 37).

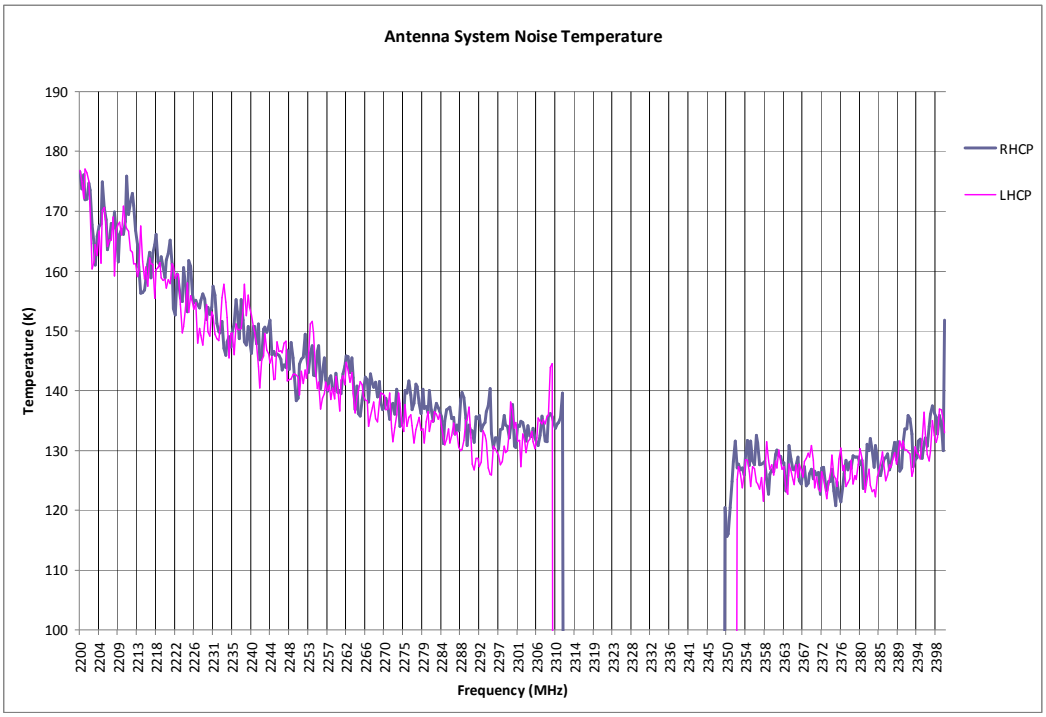

Figure 37: The antenna system noise temperature of the HSDTA.

3.5. Gain

The actual gain of the antenna array is difficult to directly measure because there are active components integrated into the feed structure for the antenna. The overall system gain was measured using a HP 8753D network analyzer. The antenna gain at mid-band, 2.3 GHz, can be interpolated from the system gain as can be seen in Table 6.

Measured Gain	45	dB
Implementation Loss:	37.29	dB
STD Gain Horn	16	dB
Est. Antenna Gain:	**23.71**	**dB**

Table 6: The Gain of the HSDTA measured at mid-band, RHCP.

Similarly, the antenna gain verse frequency was found as can be seen below in Figure 38. Across the operational band of the HSDTA, the average gain is approximately 23.4 dB.

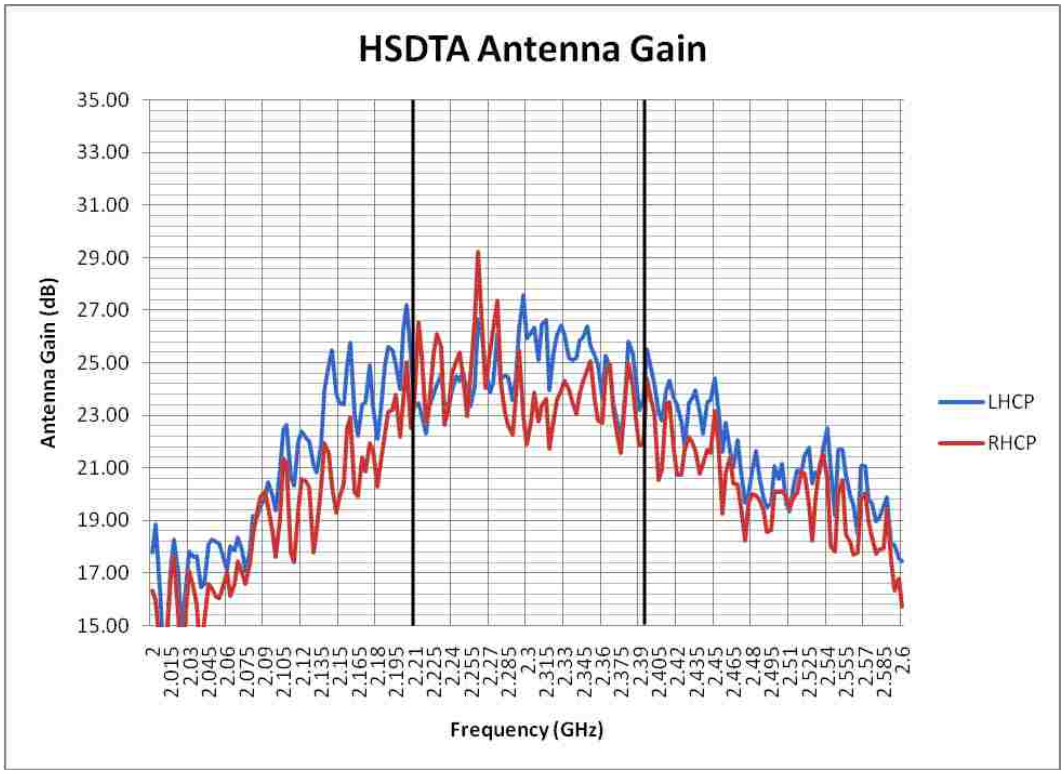

Figure 38: Gain verses frequency of the HSDTA. The desired pass-band is denoted by the bold lines.

3.6. Estimated G / T Ratio

With the gain of the antenna calculated and the antenna system noise temperature calculated, one may calculate the antenna G/T ratio by [12].

$$G/T = AntennaGain(dB) - 10\log\left(SystemNoiseTemp(K)\right) \qquad (12)$$

With the LNAs operating at 25°C and at mid-band, this calculation comes out to be 2.45 dB/K. If we were able to measure the antenna noise temperature at altitude where the LNA's noise figure drops to 0.6 dB,

lowering the system noise temperature approximately 22 K, the G/T would be ~ 3.3 dB/K.

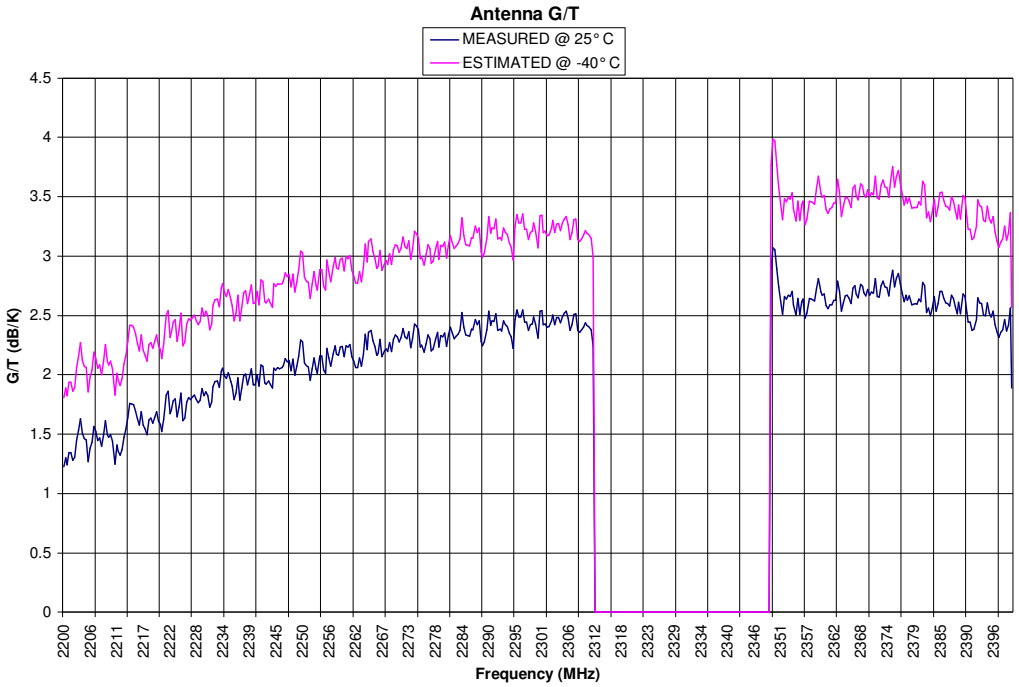

Figure 39: The measured G/T at 25° C along with the estimated G/T of the HSDTA at altitude (-40° C).

CHAPTER 4

Conclusion

An S-band aperture coupled antenna array was designed, simulated, fabricated and tested. The HSDTA is innately capable of receiving both linear polarizations. When the HSDTA is paired with a hybrid coupler, both circular polarization senses can be received. Auto-tracking is implemented through electronically scanning the quadrants of the array. The bandwidth of the HSDTA meets all design requirements. To optimize the performance of the array, the structure was simulated in CST Microwave Studio in multiple stages. The final HSDTA design can be customize for different airborne assets through the use of RF terminations to maintain the balance of the feed network when antenna elements are lost to shape the array to a specific radome profile. The HSDTA meets all design requirements listed in Section 1.3 and has been successfully operationally tested.

Throughout the process of designing, fabricating, and deploying the HSDTA, several design parameters and processes have been refined. It was found that at high altitude and after normal wear and tear, the top substrate material would tend to crack around fastener holes. This could be easily fixed by using a thicker substrate for this section of the array or by plating the holes used for fasteners. To add to the overall stiffness of the PCBs used in the HSDTA, a spray adhesive was used to adhere the foam layers to the top and backend PCBs. The adhesive was applied in a thin sheet over a large area and thus does not dramatically affect the performance of the HSDTA. By doing this, the overall rigidity of the structure was increased which is helpful in mitigating the adverse effects of long term vibration of the HSDTA.

4.1. Future Work

The HSDTA was used to collect telemetry while aboard an airborne asset flying at 35,000 ft over the South Pacific. The data quality of the telemetry collected was in close concordance with simulated data quality for an array antenna which was defined by the specification in Section 1.3.

Figure 40: The 34" HSDTA installed and ready for flight aboard a DC-8 aircraft.

Future revisions of the HSDTA may include an amplitude distribution network for each element which would allow for electronically controlled beam forming and side lobe reduction [3]. Further down the road, the HSDTA's design is ideal for implementing a large area phased array on the side of an airborne platform. This design would require both amplitude and phase control for each individual element. It could be possible to use

an additional board which was responsible for the array processing and element phasing to accomplish this.

The design and fabrication of the HSDTA has been a very fulfilling and interesting topic of research. Designing a base antenna quadrant which incurs a single Non-Recurring Engineering (NRE) charge to manufacture yet, is capable of being used for auto-tracking in at least three separate designs (all for different airborne assets), lowers cost and project risks. The final test of the HSDTA will be seen over the next few years as Ktech deploys multiple versions of the system and tests the long term survivability of the system.

References

[1] G. Deschamps, “Microstrip microwave antennas.” Presented at the 3rd USAF Symp. On Antennas, 1953.

[2] H. Gutton and G. Baissinot, “Flat Aerial for Ultra High Frequencies.” French Patent No. 703 113, 1955.

[3] D. Pozar, “Design Consideration for Low Sidelobe Microstrip Arrays.” IEEE Trans. Antennas Propaga., Vol. 38. no.8. pp1176-1185, Aug. 1990.

[4] D. Pozar, “A Microstrip Antenna Aperture Coupled to a Microstrip Line”, Electronics Letters, Vol. 21, pp.49-50, January 17, 1985.

[5] D. Pozar, **“**A Review of Aperture Coupled Microstrip Antennas: History, Operation, Development, and Applications”, May 1996.

[6] I. Bahl and P. Bhartia, *Microstrip Antennas*, Artech House, Dedham, MA, 1980.

[7] C. Balanis, *Advanced Engineering Electromagnetics*, John Wiley & Sons, New York, 1989.

[8] C. Balanis, *Antenna Theory*, John Wiley & Sons, New York, 3rd Ed,, 2005.

[9] E. Hammerstad, “Equations for Microstrip Circuit Design,” *Proc. Fifth European Microwave Conf.*, pp. 268-272, September 1975.

[10] S. Targonski and D. Pozar, “Design of wideband circularly polarized aperture coupled microstrip antennas”, IEEE Trans. Antennas and Propagation, vol. 41, pp. 214-220, February 1993.

[11] D. Pozar, “A Review of Bandwidth Enhancement Techniques for Microstrip Antennas”.

[12] Telemetry Group, Range Commanders Council (RCC), “TEST METHODS FOR TELEMETRY SYSTEMS AND SUBSYSTEMS”, Secretariat RCC, Vol. 2, June 2002

[13] W. Imbriale, “Design of a Wideband Radio Telescope”, *Aerospace Conference, 2007 IEEE*, March 2007.

[14] J. Bij de Vaate, D. Geskus, R. Witvers, “Integrated Active Antenna Noise Figure Characterization using a Cryogenic Anechoic Noise Source”, *European Microwave Conference, 2001*, October 2001.

[15] R. Pettai, *Noise in Receiving Systems*, John Wiley & Sons, New York, 1984.

[16] J. Colburn, Y. Rahmat-Samii, “Characterization of circularly polarized square cavity backed antennas”, Antennas and Propagation Society International Symposium, 1997. IEEE., Vol. 4, pp 2194-2197, July 1997.

[17] K. Wong; Wen-Hsis Hsu, "A broad-band rectangular patch antenna with a pair of wide slits”, IEEE Transactions on Antennas and Propagation, Vol. 49, Issue 9, pp. 1345-1347, September 2001.

[18] L. Lu, J.C. Coetzee, “Reduced-size microstrip patch antenna for Bluetooth applications”, IEEE Electronics Letters, Volume 41, Issue 17, pp. 944 – 945, August. 2005.

[19] W. Yazhou, S. Donglin, X. Yongxuan, “Broadband circularly polarized square microstrip antenna”, *ISAPE '06. 7th International Symposium on Antennas, Propagation & EM Theory 2006*, October 2006.

[20] R. Lee, K. Lee, K. Bobinchak, “Characteristics of a Two-Layer Electromagnetically Coupled Rectangular Patch Antenna”, IEEE Electronic Letters, September 1987.

[21] F. Rostan, W. Wiesbeck, “Aperture-coupled microstrip patch phased arrays in C- and X-band: acontribution to future multi-polarization multi-frequency SAR systems”, *IEEE International Symposium on Phased Array Systems and Technology 1996*, pp.141 – 146, October 1996.

[22] D. Pozar, B. Kaufman, “Increasing the Bandwidth of a Microstrip Antenna by Proximity Coupling”, IEEE Electronic Letters, April 1987.

[23] J. Zürcher, “The SSFIP: A Global Concept for High Performance Broadband Planar Antennas”, IEEE Electronic Letters, November 1988.

[24] R. Flagg, “Determination of G/T”, SETI League Inc., 24 Aug., 2009, <http://www.setileague.org/articles/g-t.htm>

[25] D. Pozar, "Microstrip Antennas," *Proc. IEEE*, Vol. 80, No. 1, January 1992.